FABRICATION OF BIO-BASED ACTIVATED CARBON MODIFIED GRAPHITE ELECTRODE AND ITS PERFORMANCE AS SUPERCAPACITOR

By

Md. Moniruzzaman

A THESIS SUBMITTED IN PARTIAL FULFILLMENT OF THE REQUIREMENT FOR THE DEGREE

OF

MASTER OF PHILOSOPHY (M. PHIL.) IN CHEMISTRY

Department of Chemistry

BANGLADESH UNIVERSITY OF ENGINEERING AND TECHNOLOGY

(BUET), DHAKA-1000

2022

CANDIDATE'S DECLARATION

It is hereby declared that this thesis or any part of it has not been submitted elsewhere for the award of any degree or diploma

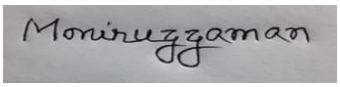

.....

(**Md. Moniruzzaman**)

Signature of the candidate

BANGLADESH UNIVERSITY OF ENGINEERING AND TECHNOLOGY (BUET), DHAKA-1000

Department of Chemistry

Certification of Thesis

A thesis on

FABRICATION OF BIO-BASED ACTIVATED CARBON MODIFIED GRAPHITE ELECTRODE AND ITS PERFORMANCE AS SUPERCAPACITOR

Submitted by

Md. Moniruzzaman, Student ID: **1018033204**, Session: October-2018, has been accepted as satisfactory in partial fulfillment of the requirements for the degree of **Master of Philosophy (M. Phil.)** in Chemistry and certify that the student has demonstrated a satisfactory knowledge of the field covered by this thesis in an oral examination held on , **2022 .**

Board of Examiners

Dr. Al-Nakib Chowdhury
Professor
Department of Chemistry
BUET, Dhaka-1000

Supervisor and Chairman

Dr. Md. Abdur Rashid
Head and Professor
Department of Chemistry
BUET, Dhaka-1000

Member (Ex-officio)

Dr. Ayesha Sharmin
Associate Professor
Department of Chemistry
BUET, Dhaka-1000

AYESHA SHARMIN

Member

Dr. Chanchal Kumar Roy
Assistant Professor
Department of Chemistry
BUET, Dhaka-1000

Member

Dr. Md. Ashaduzzaman
Professor
Applied Chemistry and Chemical Engineering
University of Dhaka, Dhaka-1000

Member (External)

Dedicated

To

My Beloved Parents

&

Honorable Supervisor

Table of Contents

List of Tables

Scheme

List of Figures

Abbreviation

Full Name	Abbreviate Name
Activated carbon	AC
Carbon nano tube	CNT
Cyclic voltammogram	CV
Electrical double layer	EDL
Electrical double layer capacitance	EDLC
Electrochemical impedance spectroscopy	EIS
Polyvinyl Alcohol	PVA
Polyvinylidine fluoride	PVDF
Carboxymethyl cellulose	CMC
Dimethyl sulfoxide	DMSO
Fourier-transform infrared spectroscopy	FT-IR
Scanning electron microscopy	SEM
Energy dispersive X-ray spectroscopy	EDS
Specific capacitance	C_s
Supercapacitor	SC

Acknowledgement

At the very beginning, I humbly express my heartiest gratitude to the almighty Allah, the most gracious, compassionate, and merciful creator, for his immeasurable mercy bestowed on me in carrying out the research work presented in the dissertation.

It gives me great pleasure to express my heartfelt gratitude, sincere indebtedness, and solemn regards to my reverend teacher and supervisor, **Dr. Al-Nakib Chowdhury**, Professor, Department of Chemistry, Bangladesh University of Engineering and Technology (BUET), for his kind supervision, invaluable guidance, valuable and constructive suggestions, liberal help, and constant encouragement during the preparation and completion of this thesis. He was important in the creation of this innovative concept, and he always advised me when I had a difficulty. He is without a doubt one of the most crucial persons in helping me convert from a greenhorn mechanical engineer to a matured, determined, autonomous, research-driven, and incredibly curious environmental engineer. It is undeniable that his contributions and efforts have had a significant impact on who I am now. In fact, I feel fortunate to be a part of his ambitious research team.

It is also my great honor to convey my sincere gratitude to my respected teacher Professor **Dr. Md. Abdur Rashid,** The honorable Head of the Department of Chemistry at BUET, for giving me his wonderful support to move through the academic processes during this M. Phil. Program. I am also momentously grateful to **Dr. Chanchal Kumar Roy**, Department of Chemistry, BUET, for his valuable and constructive suggestions, unwavering support, as well as his constant encouragement during the duration of the research period.

I would also like to acknowledge the entire department of Chemistry at Bangladesh University of Engineering and Technology, which helped me to get an overall knowledge of the field, which is imperative in doing research dealing with a real-world problem. I would like to express my deepest gratitude to all the teachers, including Professor **Dr. Md. Shakhawat Hossain Firoz**, and **Dr. Md. Nazrul Islam**, Associate Professor **Dr. Abu Bin Imran**, **Dr. Ayesha Sharmin**, Assistant professor **Dr. Sharmin Nishat**, **Dr. Md. Ayub Ali**, **Dr. Md. Abdul Goni**, **Dr. Elius Hossain,** and the Department of Chemistry, BUET, for their cordial help and encouragement during my study period and better understanding. I am highly grateful to all members of the board of examiners for their valuable suggestions and appreciate the comments. I would also like to thank all the staff of the Chemistry department in BUET for their technical support and cordial help.

I am thankful to my dear classmate and all the members of my research group for their friendly cooperation and lovely encouragement throughout my research group. Specially thanks to Akter Hossain Reaz, Md. Mahamudul Hasan, Anwarul Azim Akib, Ragib Shakil, Md. Rabiul Hasan, Keya Chowdhury, Sathi Khatun, Anila Anwar Sharmi, and all members of Advanced Research Group for their continuous help during the research.

I am thankful to the authorities of CASR BUET, the University Grants Commission (UGC) of Bangladesh, the Prime Minister's Education Assistance Trust (PMEAT), the Ministry of Science and Technology, Government of the People's Republic of Bangladesh for providing financial support for this research work.

Finally, I would like to express my heartfelt indebtedness gratitude to my beloved father, mother, brother and all of my family members for their continuous, moral supports and immeasurable sacrifices throughout my study.

08 May, 2022

Md. Moniruzzaman

Abstract

Electrochemical energy storage systems have been a focus of research in order to solve the challenge of energy storage. Supercapacitors (SCs) are energy storage devices that have distinct advantages over batteries and conventional capacitors, making them promising candidates in energy storage technology. Over the past decade, several novel electrode materials and cell designs have been studied in attempt to boost the energy density of SCs. Having porous structure, high specific surface area, superior electrical conductivity, and good chemical and thermal stability, Carboneous materials activated carbon (AC) has attracted tremendous attention for its potential applications as an electrode material or an electrode modifier in supercapacitor technologies. In this study, the modification of highly porous activated carbon (AC) electrodes fabricated from banana leaves with a series of polymeric binders like polyvinyl alcohol (PVA) and carboxymethyl cellulose (CMC), along with examining their suitability in AC-based supercapacitor applications.

To fulfill this objective, first banana leaf activated carbon (AC) was synthesized using the activated agent K_2CO_3. Furthermore, different polymeric binders were employed to analyze the electrochemical behavior of the biomass-based activated carbon supercapacitor. These composites of different binders were evaluated using scanning electron microscopy (SEM), energy dispersive X-ray spectroscopy (EDS), and Fourier-transform infrared (FT-IR) spectroscopy. The composites were deposited on a graphite substrate using binder by solution casting method. The materials were electrochemically investigated in a 0.5 M Na_2SO_4 solution using cyclic voltammetry, galvanostatic charge-discharge, and electrochemical impedance techniques to determine their capacitive behavior.The effects of binders, composite compositions, applied current density, potential scan rate, and stability were investigated in many different ways.

During the study, a greater CV curve area was exhibited for the PVA binder than for PVDF and CMC. Moreover, all of the binders' GCD curves were found to be quasi-symmetrical. However, the PVA binder showed a relatively better triangular shape and longer discharge time compared to CMC and PVDF. The specific capacitance (C_s) values of AC-PVA are generally achived to be higher than that of AC-PVDF and AC-CMC. The high Cs, power density and longer life time demonstrate that PVA binder can be a better choice as a polymer binder in AC-based supercapacitors.

CHAPTER 1

INTRODUCTION

1.1 General Remarks

Most of the present energy supply is derived from fossil fuels. However, their resources are limited and will be drained shortly [1].The huge depletion of fossil fuels on a global scale has resulted in carbon buildup in the natural cycle, where CO_2 is easily generated. CO_2 is a key contributor to greenhouse gases, which are responsible for substantial environmental changes such as global warming, flooding in the lower half of the globe, and so on [2]. In addition, the fast development of electronic equipment such as hybrid electric automobiles and portable communications technology has increased the need for high-power energy supplies [3].These concerns have been identified as one of the most pressing and significant global challenges that must be addressed. There is, therefore, a high requirement to develop alternative energy resources to meet the increasing energy demand.

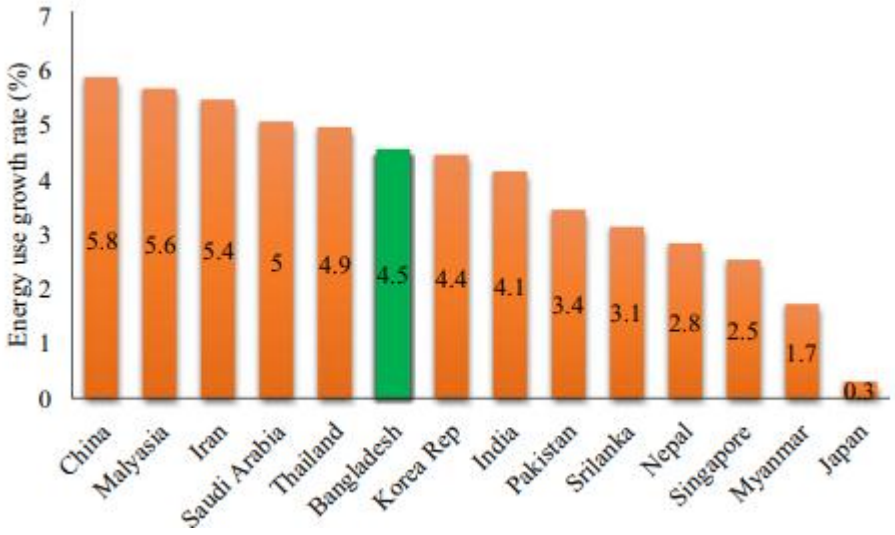

Figure 1. 1: Growth rate of energy use in different Asian countries including Bangladesh [4].

In serve this purpose, batteries are first introduced in the mid of 18th century.Since then, advances in electrical energy storage technologies have continued to accelerate, with Lithium-ion batteries reaching their pinnacle in the twenty-first century [5]. In terms of supplying power, batteries have high power density. But they are suffered from slow power density [6]. The broad usage of batteries is consequently restricted, particularly in energy-storage systems where quick charge-discharge is needed due to their poor power density.

Besides, capacitors have a higher power density. But they are suffered from lower energy density [7]. The basic mechanism of these batteries and capacitors are very similar [8-9]. It's crucial to know how capacitors and rechargeable (secondary) batteries work. A battery is made up of a positive electrode (cathode), a negative electrode (anode), and an electrolyte that permits ions to travel from the anode to the cathode during discharge and back during recharging [10]. The voltage

created between the battery terminals depends on the battery type and the chemistry involved between the electrodes and electrolytes. Figure 1.2 shows electrochemical processes and operating voltages that are typical of rechargeable batteries. The main difference between batteries and capacitors is that the former stores energy in the form of a mass of chemical reactants capable of generating charge, whilst the latter stores energy directly as surface charge.

(a)

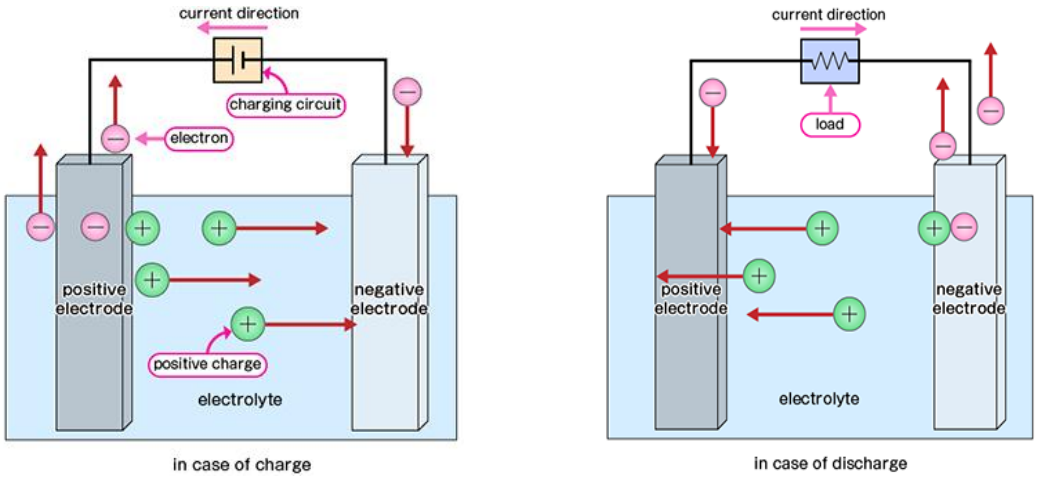

(b)

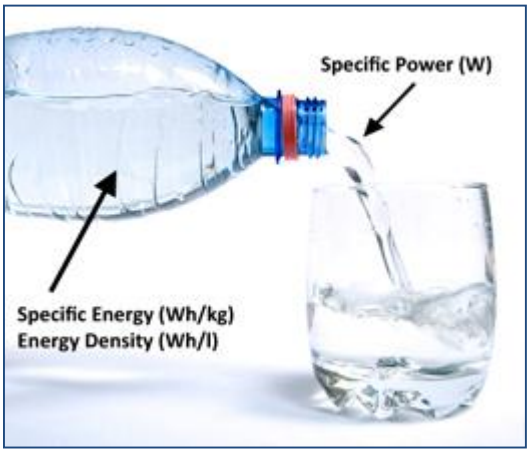

Figure 1. 2(a): Chemical reaction and electrical characteristics during charge and discharge. (b) Conceptualization of energy and 3 power density [11]

Hence, batteries have a high energy density but a low power density, while capacitors have a high power density but a low energy density. These two prominent problems can be moderated by electrochemical double layer capacitors (EDLCs), also known as supercapacitors (SCs).

Supercapacitor or ultra-capacitor is an innovative technology that fills the gap between batteries and capacitors.They provide a high specific power density (10 kW kg^{-1}), a long cycle life (> 10^5), and a quick charging-discharge process (within seconds), therefore they're gaining a lot of attraction as an alternative or substitute for batteries in the area of energy storage.

The power/energy trade-off in different charge-storage devices is represented in the so-called Ragone plot (see Figure: 1.3). Ragone plots have long been used to evaluate energy storage options with different orders of magnitude in either power or energy density [12].

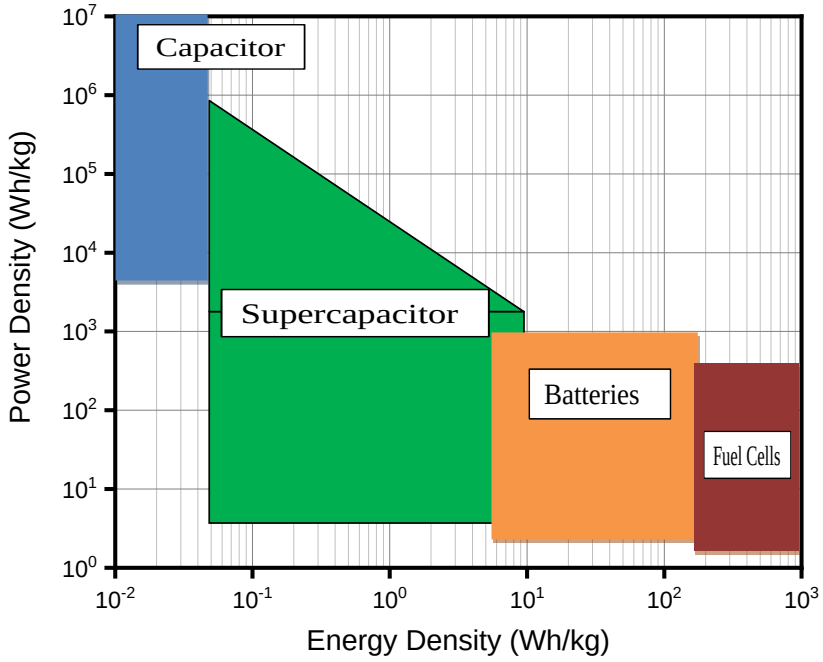

Figure 1. 3: Ragone plot for a rough comparison of energy storage technologies in terms of power or energy density.

SCs are light, thin, and conformal to some degree. These are exceptional features, particularly for smartphone devices. Instead of long-term compact energy storage, they are employed in situations where quick CD cycles are needed. By serving as dampers on power lines, SCs may help to regulate voltage variations. Supercapacitors may help stabilize the power supply in applications with changing loads such laptop computers, GPS, portable media players, and hand-held devices [13].

In order to improve the electrochemical performance of the supercapacitors, the priority challenge is not only to find new electrode materials but also to explore the other components of the device as well. Indeed, along with the electrodes, the binder appears to be another critical segment of the supercapacitor. The binders provide the required adhesion between the electrode active surface and the modifier matrices and ensure undisrupted electrical current flow throughout the device terminals [14]. The performance of the supercapacitors differs while using

a different electrode and binder material [15]. However, the use of binders may block the pore and surface sites of the electrode modifier and thus influence the electrochemical performance of the supercapacitor device [16]. In this study, we have successfully modified graphite electrode by Activeted carbon with different polymeric binder to fabricate supercapacitor electrodes with reasonable energy andpowerdensities and a high stability.

1.2 Objectives of the Work

The main objectives of the proposed research are:

I. To obtain a bio-based electro active nanostructure activated carbon (AC) from banana leaves.
II. To perform morphological and compositional studies by employing scanning electron microscopy (SEM), X-ray diffraction (XRD), and Fourier-transform infrared spectroscopy (FT-IR)
III. To modify a graphite electrode with AC for its use as the electrode modifier.
IV. To investigate the super capacitor performance with the AC modified graphite electrode using various polymeric binders.

1.3 Plan of the Present Work

The following efforts were made to achieve the goals of the objectives:

i. Activated carbon was synthesized from banana leaves.
ii. The synthesized materials were characterized by Fourier transform infrared (FT-IR) spectroscopy, scanning electron microscope (SEM) and energy dispersive spectroscopy (EDS).
iii. The prepared composites were deposited by solution casting method on a graphite electrode using PVA, PVDF and CMC as binder
iv. Electrochemical techniques such as cyclic voltammetry, Galvan static charging-discharging, and electrochemical impedance spectroscopy were carried out to investigate the capacitive behavior of these composites for supercapacitor application.

1.4 Background: On Design, Development and Techniques of Supercapacitor

1.4.1 Energy Storage Devices

There has been a hunt for effective ways to store energy on-demand since the discovery of electricity. The energy storage sector has evolved and adapted to changing energy demand and technological advancements throughout the twentieth century. Energy storage systems provide a wide range of technological solutions for managing power supply, allowing utilities and customers to develop a more resilient energy infrastructure while saving money. The battery,

capacitor, and supercapacitor (SC) are three of the most common energy storage devices outlined below.

a. Battery

Batteries are made up of one or more cells, each of which produces an electron flow in a circuit via chemical processes. An anode (the '-' side), a cathode (the '+' side), and some form of electrolyte are the three fundamental components of all batteries (a substance that chemically reacts with the anode and cathode).

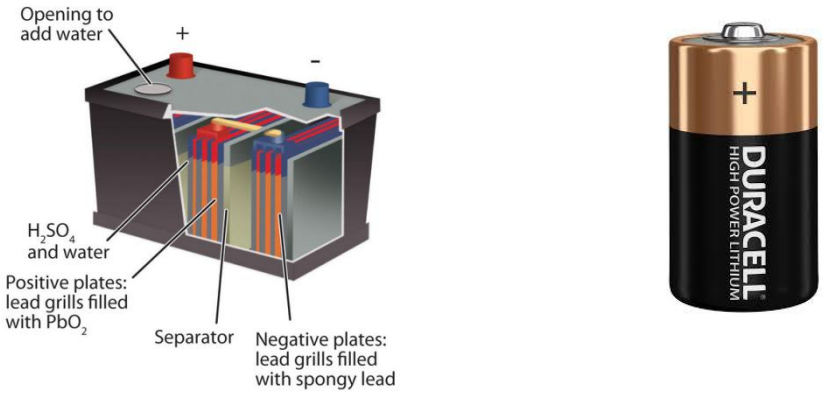

(a) (b)

Figure 1. 4 Physical outlook of different batteries (a) Lead storage battery, and (b) dry cell.

Electrolytes allow ions to travel between electrodes and terminals, allowing current to flow out of the battery and accomplish work. Charging and discharging a battery is a slow process that destroys the chemical components over time. As a result, batteries have a low power density and lose their ability to hold energy over time due to material deterioration.

b. Capacitor

Capacitors are electrical circuit components that store and filter electrical energy in the microfarad range. Capacitors include at least two electrical conductors, which are typically metal plates separated by a dielectric substance. Conductors can be made of of foil, thin sheets, sintered metal beads, or electrolytes. Dielectric materials include glass, ceramics, plastic film, paper, mica, air, and oxide layers. When an electric potential difference is applied across the terminals of a capacitor, an electric field arises across the dielectric, causing a net positive charge to accumulate on one plate and a net negative charge to accumulate on the other.

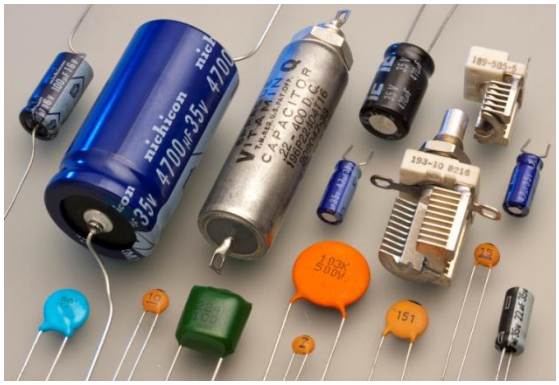

Figure 1. 5: Different capacitor's physical outlook [17]

c. Supercapacitor

Supercapacitor is energy store devices behold significant characteristics with high power density, energy density and long cycle life [18]. These energy storage devices use an electric double layer mechanism on the electrode and electrolyte surface and a psedocapacitance mechanism on the surface and near-surface to fill the gap between researchable batteries and electrochemical supercapacitors [19].It's also known as gold capacitors, electrochemical capacitors, or ultracapacitors. Supercapacitors can charge and discharge quickly due to the use of materials with a high surface area and porous and excellent conductive substances, resulting in a high-power delivery in a short period, resulting in their increased use in portable electronics, automobiles, buses, trains, cranes, and elevators due to their short charge-discharge time, which means required high power density. Supercapacitors fill the gap between batteries, which can store more energy (high energy density) but dispense it at a very slow rate. Regular electric capacitors have less energy but can quickly provide it, i.e., high-power-density [20-21].

Supercapacitors, batteries, and fuel cells are now being discarded for various purposes. Because they only differ in their charge storage systems, which determines their energy storage capacity. While supercapacitors and batteries store charge in the electrode material, fuel cells are open systems that require a source of fuel (hydrogen or methanol) and an oxidant (oxygen or air) to function [22-23]. The life cycle of a fuel cell is substantially longer than that of a battery as long as a constant supply of fuel (hydrogen, methanol, or oxygen, depending on the type of fuel cell) is maintained. Fuel cells are more appealing than batteries because of their enormous energy storage capacity, and they are used in interplanetary applications, although they are still more expensive to build. Despite the slow pace of energy distribution, the modest pathway of energy creation concept based on chemical reactions at the anode and cathode results in high energy density. Although the rate of energy delivery is not particularly impressive, the extent of battery use in day-to-day life enchanting more enticing future markets due to the modest pathway of energy generation concept based on chemical processes at the anode and cathode, resulting in high energy density. Lithium-ion batteries (LiBs) are gaining popularity in portable electronic and transportation markets due to their high energy density per unit weight or volume . Despite the significant gains recorded on Li-ion batteries, they still face considerable hurdles in cycle life and maintaining thermodynamic stability due to chemical processes that occur on the electrode/electrolyte interphase in the battery. Researchers are now concentrating on enhancing the electrode material for successful Li-ion intercalation and boosting the power density while preserving the energy storage capacity to overcome these issues [24-25]. Long cycle life and fast

charging are dependent on chemical energy stored mechanisms in the bulk of the electrode material, which is a limiting factor for increasing battery power. On the other hand, Supercapacitors store energy by charge separation and can be charged or discharged in seconds while having a long cycle life. The charge storage mechanism of supercapacitors is mostly determined by the electrode materials used in manufacturing and the fabrication method. Currently, most research is focused on finding functional materials for electrode production to increase the energy storage capabilities of supercapacitors with little or no loss in power capability [26].

1.4.2 Principle of Supercapacitor

Supercapacitors operate in the same way that electrostatic capacitors do. A traditional capacitor comprises two conductors separated by a dielectric, which is a non-conductive layer. When electrical energy is applied across the conductors, it is stored as an electrical charge that can subsequently be used as an energy source. The surface area of the conductors in supercapacitors is substantially greater than in regular capacitors.

Capacitance refers to a device's ability to store charge per unit voltage. If voltage created across the conductors is V and charge is stored in conductors ±Q, then capacitance would be

$$C=\frac{Q}{V} = \in \frac{A}{d} \qquad (1)$$

Where A is the conductors' surface area, d is the distance between the conductors, and v is the dielectric constant of the dielectric material [27-28]. Also, the stored energy (E) in a capacitor can be calculated as

$$E=\frac{1}{2}\,mV^2 \qquad (2)$$

1.4.3 Types of Supercapacitor

Supercapacitors are mainly three types: a) EDLCs b) Pseudocapacitors, and c) Hybrid Supercapacitor

a) Electrochemical Double Layer Capacitor

Rightmire initially introduced EDLCs in 1966, and they rely on capacitance derived mostly from charge separation at the electrode/electrolyte contact. There are no faradaic responses in this case.When an electrode is submerged in an electrolyte, ions pass through the porous electrode, while charges on the electrode surface spontaneously rearrange in a specific order and accumulate in the double layer primarily due to electrostatic forces, with no phase transformation in the electrode materials. The maximal charge density is accumulated at the distance of the outer Helmholtz plane, i.e., at the center of the electrostatically attracted solvated ions [29]. Because of the large interfacial area and atomic range of charge separation distances, supercapacitors based on EDLCs can store much more energy, whereas conventional capacitors store little energy due to the limited charge storage areas and geometric constraints of the separation distance between the two charged plates [30-31].

The first EDLSc model had been proposed by Helmholtz [32],

$$C_H = \frac{\in^* \in_o}{d} \quad (3)$$

Where $\in$ is the relative dielectric costant, $\in_0$ is the permittivity of empty space, and d is the distance between two parallel plates with opposing charges. The specific capacitance CH of a parallel plate capacitor is calculated using Eqn. 3, which shows that a greater relative dielectric constant and a shorter distance between the two plates may result in increased capacitance.

b) Pseudocapacitor

The faradaic process involves two types of reactions: the redox reaction in metal oxide or conducting polymer electrodes, and the adsorption of ions from the electrolyte on the electrode surface. Buzzanca and Tarasatti were the first to introduce this dual behaviour in the context of cyclic voltammetric behaviour of RuO_2 electrodes, followed by Conway et al. underpotential deposition of hydrogen ad-atom [33].

Pseudocapacitance is accompanied by an electron transfer between an electrolyte and electrode coming from a de-solvated ion. The amount of pseudocapacitance depends on the surface area, material and structure of the electrodes which contribute more capacitance than double-layer capacitance. Total capacitance (C_{total}) of a pseudocapacitor is defined by the following equation-

$$C_{total} = C_{dl} + C_{pseudo} \quad (4)$$

Here, $C_{dl}$is the double layer capacitance and $C_{pseudo}$is the pseudocapacitance of the capacitor.

The chemical affinity of carbon materials to the ion's adsorption on the electrode surface is crucial for pseudocapacitance effects (electron sorption of H or metal atoms, redox reactions of electroactive species) [34-35].

Pseudocapacitance electrodes have lower surface area dependence and often have a greater specific capacitance than standard carbon-based materials with an EDL charge storage mechanism. Surface reactions increase capacitance and improve electrochemical performance, but they also cause electrode stability to fail during cycling. Ruthenium oxide (RuO_2) has been the subject of intense research for decades because it possesses three unique oxidation states below 1.2 V, each with a high specific capacitance in acidic solutions due to pseudocapacitive behavior [36], but it is still more expensive. For less expensive and benign qualities, MnO_2, Mn_3O_4, Co_3O_4, Fe_2O_3, and NiO have been researched as RuO_2alternatives, but they never attain the same high specific capacitance as RuO_2.

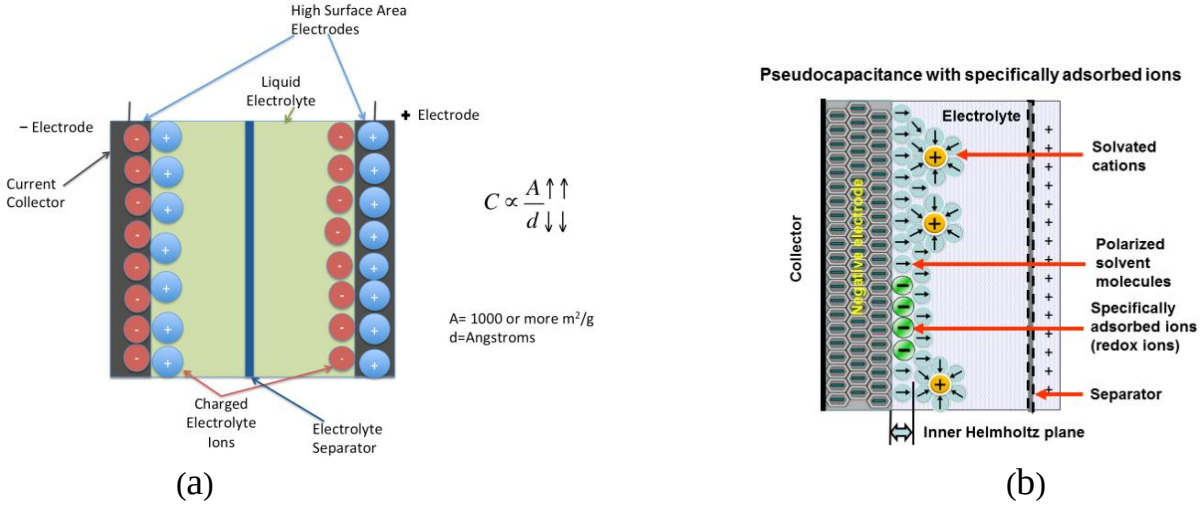

Scheme 1. 1: Schematic diagram of (a) double-layer capacitor, and (b) pseudocapacitor [37].

Pseudocapacitive materials include metal hydroxides [38], nitrides [39-40], and sulfides [41-42], which offer pseudocapacitance via surface redox processes. Conducting polymers have also been investigated as good supercapacitor electrode materials with pseudocapacitive characteristics, storing charge via bulk procedures including rapid doping and undoping to high charge densities [43].

c. Hybrid Capacitor

Hybrid supercapacitors are capacitors that have both a high capacitance and a high energy storage capacity. They've gotten a lot of attention because of their proclivity for merging the properties of their constituents (EDLC and pseudocapacitor) [44]. The possibilities for such combinations are vast, with particular interest in those produced by conducting and electroactive components and aimed at energy storage [45]. The hybrid supercapacitor, which is a mix of EDLC and pseudocapacitor, provides better performance than the individual components. The intrinsic shell area and atomic charge partition length are used to store energy in EDLC [46]. In a pseudocapacitor, energy storage is achieved through quick reproducible redox reactions among electro-active units lying atop active electrode material and an electrolyte solution [47]. The energy storage mechanism of hybrid supercapacitors is made up of the combination of these two storage techniques. Half of a hybrid supercapacitor functions as an EDLC, while the other half functions as a pseudocapacitor.In comparison to the standard EDLC and pseudocapacitor, hybrid supercapacitors have higher energy and power densities.This encourages their application in energy-efficient systems over other energy storage technologies [48]. In contrast to fuel cells and batteries, hybrid supercapacitors reach the pinnacle of power density, but have a significantly lower power density when compared to regular capacitors, as demonstrated in Fig. 1.6.

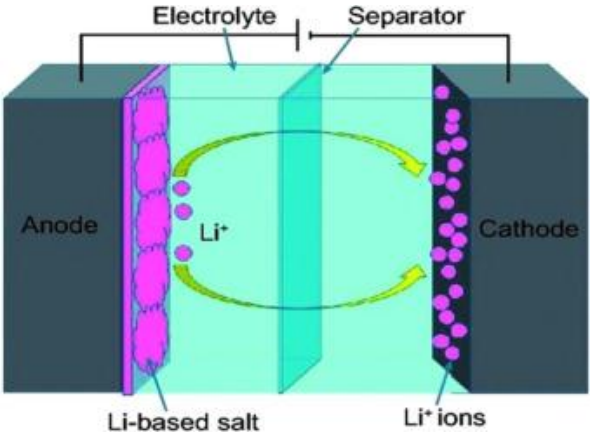

Figure 1. 6: Schematic diagram of a hybrid supercapacitor [49].

The absence of dielectric material distinguishes the supercapacitor from the normal capacitor. The traditional capacitor is made up of dielectric plates that store electrostatic charge. While a supercapacitor (hybrid) consists of submerged electrodes in an electrolyte solution separated by a separator that promotes electrolytic ion diffusion while preventing direct electrode contact or short circuit [50]. Based on two separate electrodes, the same electrodes with varying mass loadings or a mixture of two electrodes with different charge storage characteristics, hybrid supercapacitors can be asymmetric or symmetric.

1.4.4 Electrode Materials for Supercapacitor Applications

Materials for supercapacitor applications must fulfill the following requirements:

- High surface area.
- Wide working potential window
- High electrical conductivity
- Long cycle stability (>105 cycles)
- Good surface wettability

In general, three main categories of electroactive materials are used in research to fabricate SCs electrodes.

a. Carbon-based EDLC materials
b. Pseudocapacitor materials
c. Hybrid supercapacitor materials

a. Carbon-based EDLC materials

I) Graphene

A three-dimensionally (3D) stacking structure is identified as "graphite." The relevant IUPAC commission recommended the term "graphene" to replace the older term "graphite layers," which was unsuitable in the research of a single carbon layer structure because a three-dimensionally (3D) stacking structure is identified as "graphite." The most recent definition of graphene is a two-dimensional monolayer of carbon atoms that serves as the fundamental building block of graphitic materials (fullerene, nanotubes, graphite) [51]. Graphene is an elemental carbon allotrope composed of a one-atomic thick planar monolayer sheet of sp2-bonded carbon atoms

organized into a two-dimensional (2D) honeycomb crystal lattice (Fig.1.7). Graphene has a thickness of 0.34 nm. The mother of all graphitic forms is graphene.

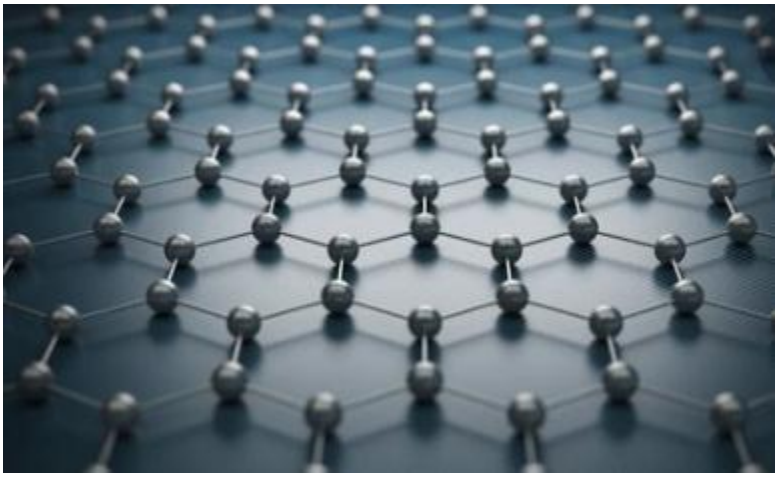

Figure 1. 7: Structure of Graphene [52].

Carbon becomes a fascinating contender due to the diversity of its allotropes and natural mass storage. Pioneering work begins with a top-down processing method, attempting to physically or chemically thin graphite [53]. Finally, in 2004, Andre Geim and Konstantin Novoselov of Manchester University succeeded in isolating singlelayer graphene using an incredibly simple mechanical exfoliation method involving only scotch tape [54] and were awarded the Nobel Prize in Physics for their groundbreaking research on graphene, a two-dimensional material found in pencil [55].It is a watershed moment for the graphene community; since then, graphene research has spread around the globe. Graphene has piqued the interest of physicists, electrical engineers, material scientists, chemists, and even biologists. Because of its remarkable thermal conductivity, outstanding mechanical strength, anomalous quantum Hall effect, and high specific surface area, this allotrope has quickly surpassed carbon nanotubes and activated carbons as the electrode material of choice for supercapacitors.

ii. Carbon nanotube (CNT)

Carbon nanotubes (CNTs) have been used as an EDLC electrode material because of its unique properties, such as excellent electric conductivity, large pore size, chemical stability, and a large specific surface area.CNTs are divided into single-walled carbon nanotubes (SWCNTs) and multi-walled carbon nanotubes (MWCNs) depending on the number of tube walls (MWCNTs). CNTs have comparable capacitive properties to ACs, however hetero-atom doped CNTs show pseudocapacitance due to a faradic reaction in the framework or functional groups on the surface.

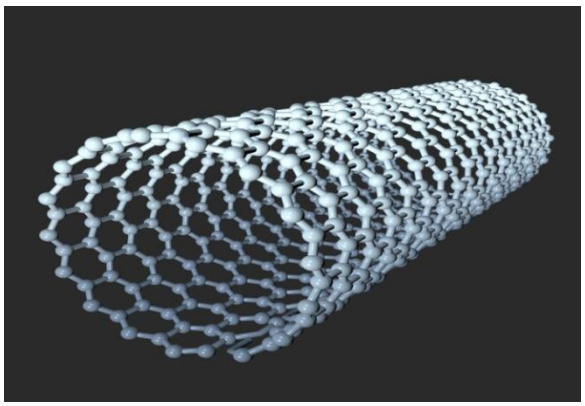

Figure 1. 8: Structure of Carbon nanotube [56].

Electronic transport occurs across long tube distances without electronic dispersion in both single and multi-walled CNTs, and the network of large exterior tiny pores generated by the CNTs' entanglement enables for rapid solvated ion diffusion during charge and discharge operations. Because of this characteristic, they can carry large current densities without wasting energy. As a consequence, CNTs are often utilized in composites; however the manufacturing costs of CNT-based supercapacitors have yet to exceed acceptable performance standards.

iii. Activated Carbon

The most common electrode material for supercapacitors is carbon. It is commonly used with a variety of variations. Because of its high surface area, low cost, ease of production in large quantities, great cycle stability, availability, wide operating temperatures, non-toxicity, and established electrode production technologies, activated carbon (AC) is the most commonly used type of porous carbon for supercapacitors. The surface area of AC in powders, woven cloths, felts, or fibers can be up to 2500 m^2 / g. In the EDLC, charge storage is largely capacitive in AC. Pseudocapacitance is also caused by surface functional groups in activated carbons that can charge and discharge [57-58]. The most often utilized ingredients for commercial AC production are coal, pitch, and petroleum coke. However, the shortage of fossil fuels, pollution concerns, and cost has prompted AC manufacturers to turn to sustainable and renewable energy. As a result, wood, nutshells, cellulose, corn grain, rice husk, banana fiber, sugar cane bagasse, and other materials are commonly used to make AC.

Figure 1. 9: Activated Carbon [59].

AC are crucial for achieving high energy density. The nature of the precursor material, the kind of activating agent, and the parameters of the activation and carbonization processes all affect the performance of porous carbons. The majority of nano porous carbons (NPCs) are made using template techniques so that the porosity and pore size may be customized. When an external potential is given to a porous carbon electrode, oppositely charged ions are absorbed on the electrode's pore surfaces, and charge buildup occurs at the electrode-electrolyte interface,

generating electric double-layers, enabling electricity to be stored [60]. As a result, they may be utilized for AC that isn't Faradic.

b. Pseudocapacitor Materials

Metal oxides such as RuO_2, TiO_2, CuO, and MnO_2 have been employed as electrode materials for pseudocapacitors because of their high conductivity [61]. Ruthenium oxide (RuO_2) has been extensively explored as an electrode material due to its high specific capacitance, strong electrical conductivity, and great thermal stability [62-64]. During the charge and discharge processes of RuO_2 based supercapacitors, a variety of redox reactions occur. The high operating potential window, variable oxidation states, highly reversible redox reactions, high proton conductivity, good thermal stability, long cycle life, metallic-type conductivity, and high rate capability encourage large-scale production of RuO_2 based SCs, but the scarcity and high cost of ruthenium (Ru) limit us. Electrode materials such as MnO_2 [65], SnO_2 [66], V_2O_5 [67], and Fe_3O_4 [68] have been used to study less costly metal oxides. Manganese oxide has been identified as a promising contender due to its nontoxicity, cheap cost, and wide availability of raw ingredients [69-72]. In 1999, Lee and colleagues reported that supercapacitors made of amorphous MnO_2nH_2O as electrode materials in a mild 2 M KCl aqueous electrolyte had an optimum specific capacitance of 200 F/g [73]. The supercapacitor using MnO_2 nanoparticles as the electrode material had a specific capacitance of around 297 F/g, which was higher than that of normal-sized MnO_2 particles. His subsequent research looked on the impact of particle size and pore size on performance [74]. This provides a mechanism for altering the particle size and porosity structure of MnO_2 particles to optimize their electrochemical performance.

c. Hybrid Supercapacitor Materials

Hybrid electrochemical capacitors with a double-layer carbon material and a pseudocapacitance material have gotten a lot of attention [75]. The capacitance of hybrid supercapacitors is made up of two layers of capacitance: double-layer capacitance stored in porous carbon materials and pseudocapacitance stored in metal oxide or conducting polymer. Hybrid supercapacitors were created to combine the benefits of EDLCs and pseudocapacitors while resolving the majority of their drawbacks.

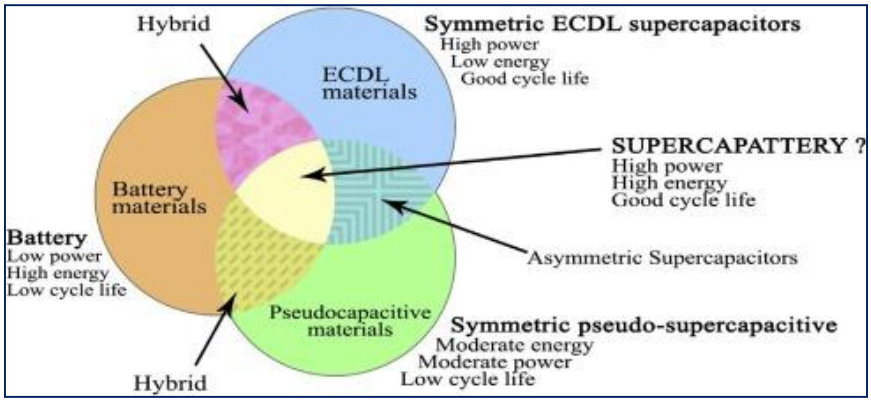

Figure 1. 10: Hybrid Supercapacitor Materials [76].

1.5. Binders for Supercapacitors

Binders are a critical component of supercapacitor electrodes and are essential for more sustainable and "green" electrode manufacturing. Binders' major function is to serve as an efficient dispersion agent, binding the electrode species together and then adhering them to the current collectors in a steady manner, allowing for optimum electron flow contact [77]. Due to their outstanding electrochemical and thermal stability, as well as strong adhesion between the current collectors and electrode sheets, polyvinyl alcohol (PVA), carboxymethyl cellulose (CMC), and polyvinylidene fluoride (PVdF) are the most often used binder for electrode materials in supercapacitors [78].

1.5.1 Types of Commercial Binders for Supercapacitors

Different types of binders used for SC are organic binders, Functionalized Polymeric Binders, and Unfuctionalized Polymeric Binders. In this study, we use PVA, PVDF, and CMC.

i. Polyvinyl Alcohol (PVA)

PVA is a low-cost synthetic polymer with great adhesive qualities that is commercially accessible. PVA has been studied as a functional polymer binder for strong hydrogen bonding, decrease capacity degradation and increasing cathode cycle life [79]. PVA has a valuable polysulfide entrapping capacity and a substantially greater binding strength when compared to traditional binder polyvinylidene fluoride. To increase electrode material adhesion, PVA is predicted to generate a strong hydrogen bond with both the current collector and active components [79]. Because hydroxyl groups may establish extremely strong hydrogen bonds with

both active materials and the current collector, a PVA containing multiple hydroxyl groups might be an excellent candidate as a binder for high capacity anodes [80].

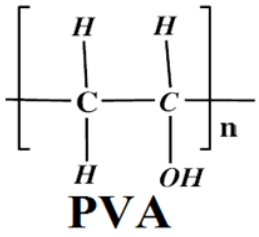

Figure 1. 11: Chemical structure of PVA

PVA might be a new binder for high-capacity anodes since it is water-soluble, non-toxic, semicrystalline, biocompatible, and biodegradable. The PVA binder will greatly improve the electrochemical characteristics of high-capacity anodes by integrating technologies to make high-capacity active materials [81].

ii. Polyvinylidene fluoride (PVDF)

Polyvinylidene fluoride is the most common sulfur cathode binder (PVDF). It bonds the active materials together like "glue" and connects the conductive networks to the current collector at a sulfur loading density of 2 mg/cm^{-2}.It lacks the ability to entrap the intermediate lithium polysulfide species and hence inhibit "polysulfide shuttling." PVDF is an excellent host binder because it is made up of CH_2-CF_2 repeating units [82]. It has good thermal stability, chemical resistance, biodegradability, and film-forming ability, thus it may be employed in a variety of applications [83].

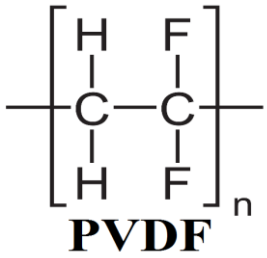

Figure 1. 12: Chemical structure of PVDF

In this area, functional binders with enhanced polysulfide trapping capabilities have sparked a lot of attention as a way to produce sulfur cathodes with better capacity retention.

iii. Carboxymethyl cellulose (CMC)

Carboxymethyl cellulose (CMC) is produced by the insertion of carboxymethyl groups in natural cellulose [84]. It is a commercially available binder that is very eco-friendly in nature because it

does not contain any fluorine in the polymer chain and can increase the dispersion stability of graphite slurry [85]. The mechanical properties of CMC are dependent on its molecular weight (MW), which influences the solubility and viscosity of its water solutions. It is widely accepted that the binder functional group density can significantly influence the cycling of electrodes [86]. In addition, CMC binder plays an additional role as a surface modifier which reduces surface resistances by forming passivation layers [87]. These properties were determined by 1) values of degree of substitution, 2) lengths of a polymeric chain, and 3) types of counter ions.

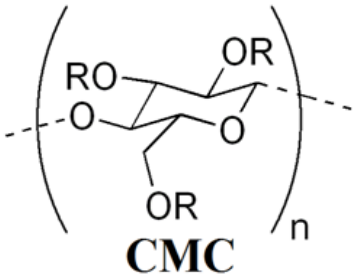

Figure 1. 13: Chemical structure of CMC

1.5.2 Binding Mechanism

Binder is responsible for particle adhesion and binding of the electrode composite to the current collectors [88] . The inherent features of polymeric bonders, such as component elements, chain length, and crystallinities, were altered by the binding activity. The conformation, which depicts the size and shape of the distributed polymer in the liquids, is determined by these parameters. Furthermore, different functional groups of polymers may create chemical interactions with active materials and current collectors, such as hydrogen bonds and covalent bonds, resulting in increased electrode adhesion forces.

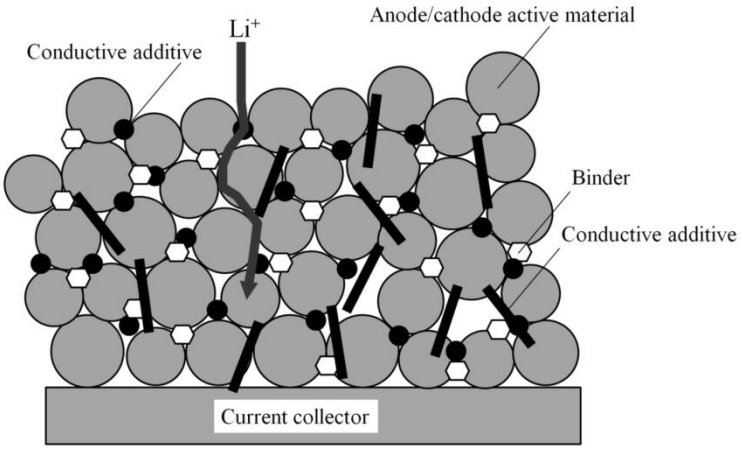

Figure 1. 14: Chemical bond between binder and current collector [89].

1.6. Electrolytes for Supercapacitors

The electrolyte used in a supercapacitor has a significant impact on its capacitance. Several electrolytes have been developed and studied based on the nature of the electrolyte, such as ion type and size, ion concentration and solvent, ion-solvent interaction, ion-electrolyte contact, ion-electrolyte interaction [90]. As a result, an ideal electrolyte should have a broad voltage window, high conductivity, great electrochemical stability, small solvated ionic radius, high ionic concentration, low viscosity, high purity, be environmentally acceptable, inexpensive in cost, and widely accessible. Organic, aqueous, and ionic liquid electrolytes have been utilized with activated carbon electrodes

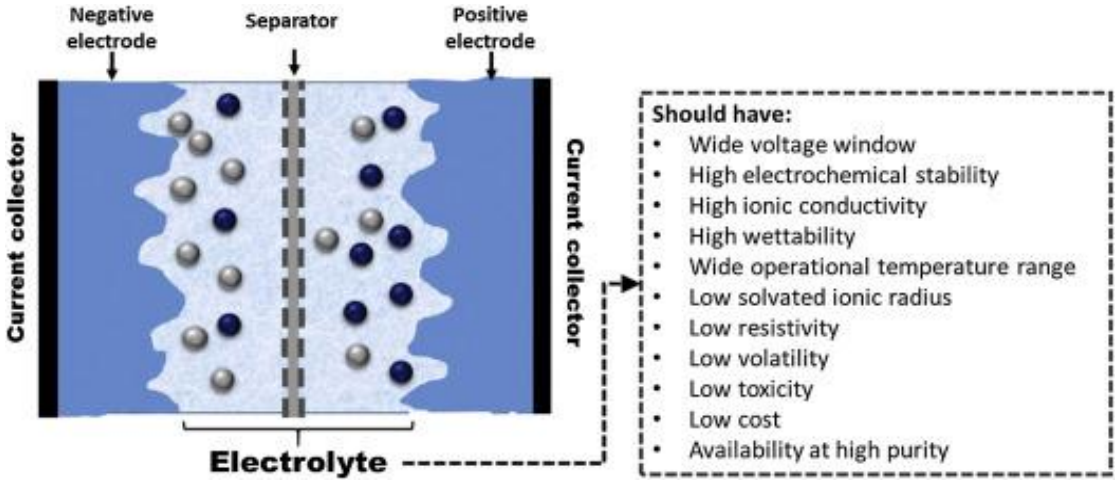

Figure 1. 15: Electrolyte for electrochemical supercapacitor [91].

1.7. Experimental Techniques for Supercapacitors

1.7.1. Cyclic Voltammetry

The most comprehensive electroanalytical approach for the investigation of electroactive substances is cyclic voltammetry [92]. It's become a popular method for beginning electrochemical research of experimental systems. It's been quite helpful in obtaining data on some rather complex electrode responses.

In the CV experiment, an enclosed, stationary electrode is scanned from a beginning potential to a final potential, which is known as the ‘switching potential.' After that, a reverse scan for the same possible range is done. This results in a "cyclic" sweep of potentials that may be repeated as needed. The cyclic voltammogram (CV) curve is defined by the current vs. potential curve produced from the data. The potential extreme ends are termed the ' scan window' whereas first sweep is called the ' forward scan' and the return wave is called the ' reverse scan'.When the voltage is increased, the first current response is capacitive because the electrical double layer (EDL) that grows on the electrode surface is diffusion-controlled. This is how the EDL is formed. When the potential reaches a particular value that favors the reduction of the active material, the current response increases quickly, resulting in an anodic peak and the current and potential associated with it are referred to as anodic peak current and anodic potential [93]. After reaching the maximum rate of mass transfer, the current begins to decrease and continues to fall until it reaches equilibrium at a constant value. A similar but opposite peak current may be detected when potential reaches a value that promotes oxidation of the reduced species on its path back to the original value.

$$\mathbf{R + e^{-} \leftrightarrow O} \qquad (5)$$

The fundamental equation that relates the potential (E) and concentration is the Nernst equation—

$$E = E_o + \frac{0.059}{n} \log \left[\frac{C_0}{C_R}\right] \qquad (6)$$

One of the most remarkable features of CV is that the total current rises as the scan rate increases. The scan rate is defined as the pace at which potential changes over time. The diffusion layer's size, as well as the time it took to capture the scan, might be utilized to justify it.

1.7.2 Galvanostatic charge-discharge

Chronopotentiometry is the most typical constant current experiment (CP). It's an electro-analytical method in which a constant current is applied to the working electrode and the resulting potential is measured as a function of time against a reference electrode. The internal resistance (IR) created by the fast discharge of reactant from the electrode surface causes the measured potential to fluctuate quickly [94]. The graphs that appear illustrate the current excitation signal and potential response as a function of time. The GCD may be used to identify the kind of electrode material. In CP, for example, the potential response of a perfect capacitive material shows a discharge/charge time of 1 that can be easily seen.

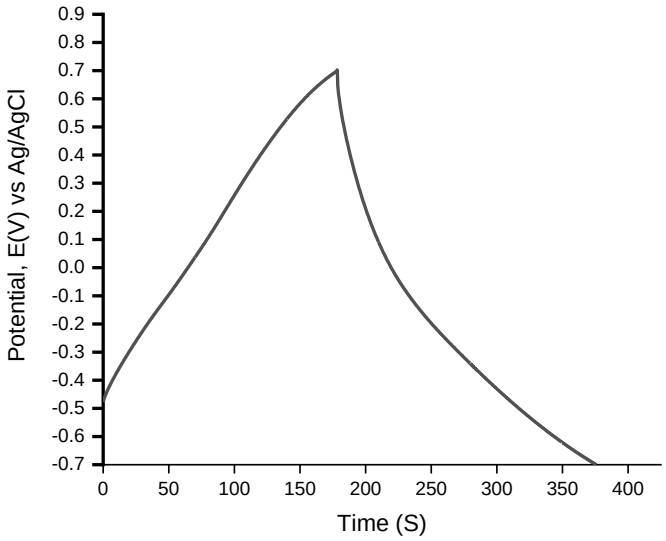

Figure 1. 16: A typical charge-discharge curve.

The specific capacitance of an electrochemical capacitor can be easily calculated from its potential response in GCD on the basis of the following equation [95]

$$C_{sp} = \frac{i\Delta t}{m\Delta V} \qquad (7)$$

Where C_{sp} stands for specific capacitance, I for discharge current (cathodic current), m for active electrode material mass, t for total discharge duration, and V for potential drop during discharge.

1.7.3 Electrochemical Impedance Spectroscopy (EIS)

Electrochemical impedance is a characteristic that describes electronic circuits, components, and the materials used to produce those components [96]. The complex variable impedance (Z) is

visually represented on a vector plane. It is defined as the overall resistance of a device or circuit to the passage of an alternate current (AC) at a certain frequency [97]. EIS is a technique for creating a direct connection between a real system and an idealized equivalent circuit made up of discrete electrical components in series and parallel configurations (resistance, capacitor, and inductor). Blocking or polarizable electrodes (in the case of EDLC, planar geometries or large surface area porous electrodes) or electroactive electrode materials are used in electrochemical capacitors (in the case of redox capacitors).

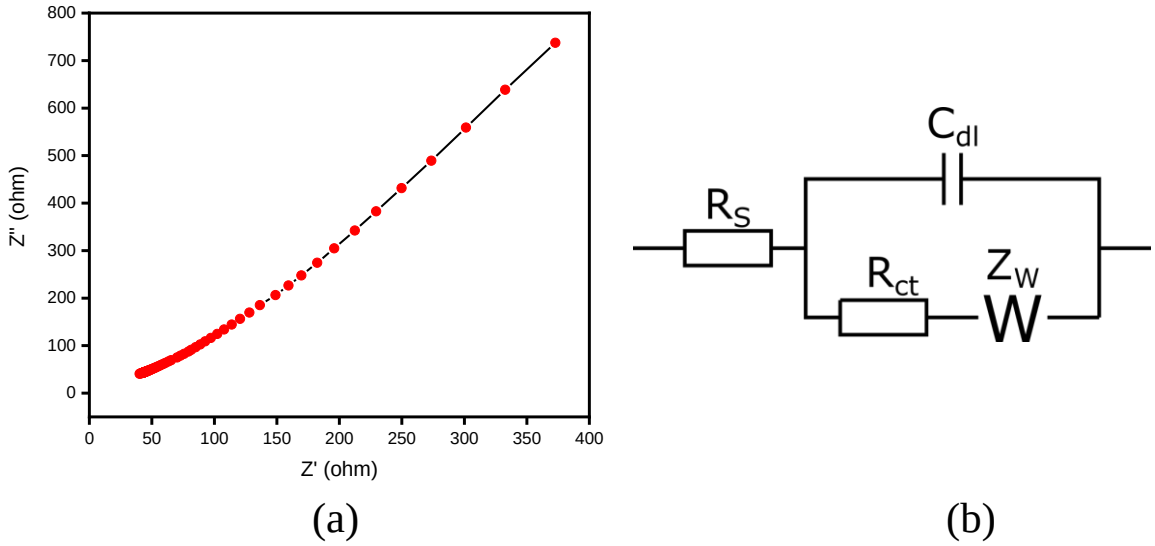

Figure 1. 17: (a) and (b) its equivalent circuit [98].

EIS permits for the diagnostics as well as the implementation of electrochemical procedures [99]. It is feasible to determine the type of an electroactive substance using EIS. It's been used in engineering, biosensor applications, and other fields.

1.7.4 Evaluation of Electrode

Various characterization and measurement can be carried out on activated carbon for the purpose of supercapacitor electrodes. The structure and morphology of AC materials, for example, are studied using scanning electron microscopy (SEM). Energy dispersive X-ray spectroscopy (EDX) was used to assess the specimen's chemical composition, and FTIR was used to analyze the sample's surface chemistry and the presence of functional groups. Electrochemical measuring electrode testing may be done using two or three-electrode setups. The three-electrode assembly employs electrochemical impedance spectroscopy (EIS) for ion transport mechanisms, galvanostatic charge-discharge (GCD), also known as chronopotentiometry (CP), for charge storage mechanisms, and cyclic voltammetry (CV) for thermodynamics of the system's electrochemical reactions [100].

References:

[1] Heede, R., and Oreskes, N., "Potential emissions of CO_2 and methane from proved reserves of fossil fuels: An alternative analysis," *Glob. Environ. Chang.*, vol. 36, pp. 12–20, 2016.

[2] Anderson, T. R., Hawkins, E., and Jones, P. D., "CO_2, the greenhouse effect and global warming: from the pioneering work of Arrhenius and Callendar to today's Earth System Models," *Endeavour*, vol. 40, no. 3, pp. 178–187, Sep. 2016.

[3] Bose, B. K., "Global warming: Energy, environmental pollution, and the impact of power electronics," *IEEE Ind. Electron. Mag.*, vol. 4, no. 1, pp. 6–17, Mar. 2010.

[4] Washim Akram, M., Arman M. A., and Nusrat, A., "Prospect of green power generation as a solution to energy crisis in Bangladesh," *Energy Systems*. Springer Science and Business Media Deutschland GmbH, pp. 1–39, Jan. 2021.

[5] Xin, S., Gao, H., Li, Y., and Guo, Y.-G., *Nanostructures and Nanomaterials for Batteries*. Singapore: Springer Singapore, 2019.

[6] Li. J *et al.*, "Toward Low-Cost, High-Energy Density, and High-Power Density Lithium-Ion Batteries," *JOM*, vol. 69, no. 9. Minerals, Metals and Materials Society, pp. 1484–1496, Sep. 2017.

[7] Wang, Y., Song, Y., and Xia, Y., "Electrochemical capacitors: Mechanism, materials, systems, characterization and applications," *Chemical Society Reviews*, vol. 45, no. 21. Royal Society of Chemistry, pp. 5925–5950, Nov. 2016.

[8] Zheng, J. P., and Jow, T. R., "High energy and high power density electrochemical capacitors," *J. Power Sources*, vol. 62, no. 2, pp. 155–159, Oct. 1996.

[9] Miller, J. R., and Burke, A. F., "Electrochemical capacitors: Challenges and opportunities for real-world applications," *Electrochem. Soc. Interface*, vol. 17, no. 1, pp. 53–57, Mar. 2008.

[10] Pavkovic, D., Lobrovic, M., Hrgetic, M., Komljenovic, A., and Smetko, V., "Battery current and voltage control system design with charging application," in *2014 IEEE Conference on Control Applications, CCA. Part of 2014 IEEE Multi-conference on Systems and Control, MSC* Dec. 2014, pp. 1133–1138, *2014*.

[11] Hanrahan. B *et al.*, "A Portable Power Concept Based on Combustion and Pyroelectric Energy Conversion," *Cell Rep. Phys. Sci.*, vol. 1, no. 6, p. 100075, Jun. 2020.

[12] Raut, A. S., Parker, C. B., and Glass, J. T., "A method to obtain a Ragone plot for evaluation of carbon nanotube supercapacitor electrodes," *J. Mater. Res.*, vol. 25, no. 8, pp. 1500–1506, Aug. 2010.

.

[13] Shi, Y., Zhou, X., and Yu, G., "Material and Structural Design of Novel Binder Systems for High-Energy, High-Power Lithium-Ion Batteries," *Acc. Chem. Res.*, vol. 50, no. 11, pp. 2642–2652, Nov. 2017.

[14] J. Gomez and E. E. Kalu, "High-performance binder-free Co-Mn composite oxide supercapacitor electrode," *J. Power Sources*, vol. 230, pp. 218–224, 2013.

[15] Z. Zhu *et al.*, "Effects of various binders on supercapacitor performances," *Int. J. Electrochem. Sci.*, vol. 11, no. 10, pp. 8270–8279, 2016.

[16] C. Luo, Y. Zhu, Y. Wen, J. Wang, and C. Wang, "Carbonized Polyacrylonitrile- Stabilized SeS_x Cathodes for Long Cycle Life and High Power Density Lithium Ion Batteries," *Adv. Funct. Mater.*, vol. 24, no. 26, pp. 4082–4089, Jul. 2014.

[17] R. Kötz and M. Carlen, "Principles and applications of electrochemical capacitors," *Electrochim. Acta*, vol. 45, no. 15–16, pp. 2483–2498, May 2000.

[16] B. Zhao *et al.*, "A high-energy, long cycle-life hybrid supercapacitor based on graphene composite electrodes," *Energy Storage Mater.*, vol. 7, pp. 32–39, Apr. 2017.

[17] S. Banerjee *et al.*, "Capacitor to supercapacitor," in *Springer Series in Materials Science*, vol. 300, Springer, pp. 53–89, 2020.

[18] C. Portet, P. L. Taberna, P. Simon, E. Flahaut, and C. Laberty-Robert, "High power density electrodes for Carbon supercapacitor applications," *Electrochim. Acta*, vol. 50, no. 20, pp. 4174–4181, Jul. 2005..

[19] X. He *et al.*, "Efficient preparation of biomass-based mesoporous carbons for supercapacitors with both high energy density and high power density," *J. Power Sources*, vol. 240, pp. 109–113, Oct. 2013.

[20] D. P. Dubal, O. Ayyad, V. Ruiz, and P. Gómez-Romero, "Hybrid energy storage: The merging of battery and supercapacitor chemistries," *Chemical Society Reviews*, vol. 44, no. 7. Royal Society of Chemistry, pp. 1777–1790, Apr. 2015..

[21] C. Y. Wang, "Fundamental models for fuel cell engineering," *Chem. Rev.*, vol. 104, no. 10, pp. 4727–4765, Oct. 2004..

[22] B. K. Saikia, S. M. Benoy, M. Bora, J. Tamuly, M. Pandey, and D. Bhattacharya, "A brief review on supercapacitor energy storage devices and utilization of natural carbon resources as their electrode materials," *Fuel*, vol. 282. Elsevier Ltd, Dec. 2020.

[23] A. M. Divakaran *et al.*, "Rational design on materials for developing next generation lithium-ion secondary battery," *Progress in Solid State Chemistry*, vol. 62. Elsevier Ltd, p. 100298, Jun. 2021.

[24] A. Khaligh and Z. Li, "Battery, ultracapacitor, fuel cell, and hybrid energy storage systems for electric, hybrid electric, fuel cell, and plug-in hybrid electric vehicles: State of

the art," *IEEE Trans. Veh. Technol.*, vol. 59, no. 6, pp. 2806–2814, Jul. 2010.

[25] S. P. Ong *et al.*, "Voltage, stability and diffusion barrier differences between sodium-ion and lithium-ion intercalation materials," *Energy Environ. Sci.*, vol. 4, no. 9, pp. 3680–3688, Sep. 2011.

[26] Q. Ma, Y. Yu, M. Sindoro, A. G. Fane, R. Wang, and H. Zhang, "Carbon-Based Functional Materials Derived from Waste for Water Remediation and Energy Storage," *Advanced Materials*, vol. 29, no. 13. Wiley-VCH Verlag, Apr. 2017.

[27] D. Slawig, L. Rizzi, T. Rothe, J. Schuster, and C. Tegenkamp, "Anisotropic transport properties of graphene-based conductor materials," *J. Mater. Sci.*, vol. 56, no. 26, pp. 14624–14631, Sep. 2021.

[28] R. L. Spyker, "Classical equivalent circuit parameters for a double-layer capacitor," *IEEE Trans. Aerosp. Electron. Syst.*, vol. 36, no. 3 PART 1, pp. 829–836, 2000.

[29] E. González-Tovar, F. Jiménez-Ángeles, R. Messina, and M. Lozada-Cassou, "A new correlation effect in the Helmholtz and surface potentials of the electrical double layer," *J. Chem. Phys.*, vol. 120, no. 20, pp. 9782–9793, May 2004.

[30] D. C. Grahame, "The electrical double layer and the theory of electrocapillarity," *Chem. Rev.*, vol. 41, no. 3, pp. 441–501, Dec. 1947.

[31] C. Lei, F. Markoulidis, Z. Ashitaka, and C. Lekakou, "Reduction of porous carbon/Al contact resistance for an electric double-layer capacitor (EDLC)," *Electrochim. Acta*, vol. 92, pp. 183–187, Mar. 2013.

[32] W. Hsieh, T.-L. A. Horng, H.-C. Huang, and H. Teng, "Facile simulation of carbon with wide pore size distribution for electric double-layer capacitance based on Helmholtz models," *J. Mater. Chem. A*, vol. 3, no. 32, pp. 16535–16543, Aug. 2015.

[33] B. E. Conway, V. Birss, and J. Wojtowicz, "The role and utilization of pseudocapacitance for energy storage by supercapacitors," *J. Power Sources*, vol. 66, no. 1–2, pp. 1–14, 1997.

[34] Z. Song *et al.*, "Self- Assembled Carbon Superstructures Achieving Ultra- Stable and Fast Proton- Coupled Charge Storage Kinetics," *Adv. Mater.*, vol. 33, no. 49, p. 2104148, 2021.

[35] G. Lota, K. Fic, and E. Frackowiak, "Carbon nanotubes and their composites in electrochemical applications," *Energy Environ. Sci.*, vol. 4, no. 5, pp. 1592–1605, 2011.

[36] C. Yang *et al.*, "Flexible highly specific capacitance aerogel electrodes based on cellulose nanofibers, carbon nanotubes and polyaniline," *Electrochim. Acta*, vol. 182, pp. 264–271, 2015.

[37] L. Zhang, J. Wang, J. Zhu, X. Zhang, K. San Hui, and K. N. Hui, "3D porous layered double hydroxides grown on graphene as advanced electrochemical pseudocapacitor materials," *J. Mater. Chem. A*, vol. 1, no. 32, pp. 9046–9053, 2013.

[38] R. M. Obodo *et al.*, "Recent advances in metal oxide/hydroxide on three-dimensional nickel foam substrate for high performance pseudocapacitive electrodes," *Curr. Opin. Electrochem.*, vol. 21, pp. 242–249, 2020.

[39] C. Yi, J. Zou, H. Yang, and L. Xian, "Recent advances in pseudocapacitor electrode materials: transition metal oxides and nitrides," *Trans. Nonferrous Met. Soc. China*, vol. 28, no. 10, pp. 1980–2001, 2018.

[40] K. Robert *et al.*, "Novel insights into the charge storage mechanism in pseudocapacitive vanadium nitride thick films for high-performance on-chip micro-supercapacitors," *Energy Environ. Sci.*, vol. 13, no. 3, pp. 949–957, 2020.

[41] K. Krishnamoorthy, P. Pazhamalai, and S. J. Kim, "Ruthenium sulfide nanoparticles as a new pseudocapacitive material for supercapacitor," *Electrochim. Acta*, vol. 227, pp. 85–94, 2017.

[42] G. Fang *et al.*, "Observation of pseudocapacitive effect and fast ion diffusion in bimetallic sulfides as an advanced sodium- ion battery anode," *Adv. Energy Mater.*, vol. 8, no. 19, p. 1703155, 2018.

[43] S. Chen, K. Li, K. S. Hui, and J. Zhang, "Regulation of lamellar structure of vanadium oxide via polyaniline intercalation for high- performance aqueous zinc- ion battery," *Adv. Funct. Mater.*, vol. 30, no. 43, p. 2003890, 2020.

[44] N. R. Chodankar *et al.*, "True meaning of pseudocapacitors and their performance metrics: asymmetric versus hybrid supercapacitors," *Small*, vol. 16, no. 37, p. 2002806, 2020.

[45] D. P. Dubal, O. Ayyad, V. Ruiz, and P. Gomez-Romero, "Hybrid energy storage: the merging of battery and supercapacitor chemistries," *Chem. Soc. Rev.*, vol. 44, no. 7, pp. 1777–1790, 2015.

[46] A. Muzaffar, M. B. Ahamed, K. Deshmukh, and J. Thirumalai, "A review on recent advances in hybrid supercapacitors: Design, fabrication and applications," *Renew. Sustain. Energy Rev.*, vol. 101, pp. 123–145, 2019.

[47] A. Borenstein, O. Hanna, R. Attias, S. Luski, T. Brousse, and D. Aurbach, "Carbon-based composite materials for supercapacitor electrodes: a review," *J. Mater. Chem. A*, vol. 5, no. 25, pp. 12653–12672, 2017.

[48] Y. Zhang *et al.*, "Realizing both high energy and high power densities by twisting three carbon- nanotube- based hybrid fibers," *Angew. Chemie Int. Ed.*, vol. 54, no. 38, pp. 11177–11182, 2015.

[49] X. Wu, Z.-B. Zhai, K.-J. Huang, R.-R. Ren, and F. Wang, "Boosting energy and power performance of aqueous energy storage by engineering ultra-fine metallic VSe2 nanoparticles anchored reduced graphene oxide," *J. Power Sources*, vol. 448, p. 227399, 2020.

[50] Z. Liu *et al.*, "Safer Lithium- ion batteries from the separator aspect: development and future perspectives," *Energy Environ. Mater.*, vol. 4, no. 3, pp. 336–362, 2021.

[51] R. B. Rakhi, N. A. Alhebshi, D. H. Anjum, and H. N. Alshareef, "Nanostructured cobalt sulfide-on-fiber with tunable morphology as electrodes for asymmetric hybrid supercapacitors," *J. Mater. Chem. A*, vol. 2, no. 38, pp. 16190–16198, 2014.

[52] V. Singh, D. Joung, L. Zhai, S. Das, S. I. Khondaker, and S. Seal, "Graphene based materials: past, present and future," *Prog. Mater. Sci.*, vol. 56, no. 8, pp. 1178–1271, 2011.

[53] L. W. T. Ng *et al.*, *Printing of Graphene and Related 2D Materials*. Springer, 2019.

[54] F. Pulizzi, O. Bubnova, S. Milana, D. Schilter, D. Abergel, and A. Moscatelli, "Graphene in the making," *Nat. Nanotechnol.*, vol. 14, no. 10, pp. 914–918, 2019.

[55] A. C. Ferrari *et al.*, "Science and technology roadmap for graphene, related two-dimensional crystals, and hybrid systems," *Nanoscale*, vol. 7, no. 11, pp. 4598–4810, Mar. 2015..

[56] H. Pan, J. Li, and Y. P. Feng, "Carbon nanotubes for supercapacitor," *Nanoscale Res. Lett.*, vol. 5, no. 3, pp. 654–668, Mar. 2010.

[57] X. R. Li *et al.*, "Effect of the oxygen functional groups of activated carbon on its electrochemical performance for supercapacitors," *New Carbon Mater.*, vol. 35, no. 3, pp. 232–243, Jun. 2020.

[58] D. Qu, "Studies of the activated carbons used in double-layer supercapacitors," *J. Power Sources*, vol. 109, pp. 403–411, 2002.

[59] Y. Gao, Q. Yue, B. Gao, and A. Li, "Insight into activated carbon from different kinds of chemical activating agents: A review," *Sci. Total Environ.*, vol. 746, p. 141094, Dec. 2020.

[60] F. Béguin, V. Presser, A. Balducci, and E. Frackowiak, "Carbons and electrolytes for advanced supercapacitors," *Adv. Mater.*, vol. 26, no. 14, pp. 2219–2251, Apr. 2014.

[61] T. E. Balaji, H. Tanaya Das, and T. Maiyalagan, "Recent Trends in Bimetallic Oxides and Their Composites as Electrode Materials for Supercapacitor Applications," *ChemElectroChem*, vol. 8, no. 10, pp. 1723–1746, May 2021.

[62] L. Y. Chen, Y. Hou, J. L. Kang, A. Hirata, T. Fujita, and M. W. Chen, "Toward the Theoretical Capacitance of RuO2 Reinforced by Highly Conductive Nanoporous Gold," *Adv. Energy Mater.*, vol. 3, no. 7, pp. 851–856, Jul. 2013.

[63] Z. S. Wu *et al.*, "Anchoring Hydrous RuO2 on Graphene Sheets for High-Performance Electrochemical Capacitors," *Adv. Funct. Mater.*, vol. 20, no. 20, pp. 3595–3602, Oct. 2010.

[64] D. Majumdar, T. Maiyalagan, and Z. Jiang, "Recent Progress in Ruthenium Oxide-Based Composites for Supercapacitor Applications," *ChemElectroChem*, vol. 6, no. 17, pp. 4343–4372, Sep. 2019..

[65] P. Anandhi, V. Jawahar Senthil Kumar, and S. Harikrishnan, "Preparation and enhanced capacitive behavior of Ni-ZnO nanocomposite as electrode for supercapacitor," *Mater. Today Proc.*, vol. 9, pp. 361–370, Jan. 2019.

[66] D. Sud, "Sol-gel synthesis of transition metal oxides based electrode materials for supercapacitors," *Mater. Res. Found.*, vol. 24, pp. 155–185, Jan. 2018.

[67] S. Fleischmann, I. Kamboj, and V. Augustyn, "Nanostructured Transition Metal Oxides for Electrochemical Energy Storage," *Transit. Met. Oxides Electrochem. Energy Storage*, pp. 183–212, Jun. 2022.

[68] D. C. Sekhar, B. S. Diwakar, B. R. Babu, and N. Madhavi, "Development of graphene oxide based hybrid metal oxide nanocomposites of GO-SnO2/ZnO/Fe3O4, GO-SiO2/ZnO/Fe3O4 for energy applications," *Phys. B Condens. Matter*, vol. 603, p. 412749, Feb. 2021.

[69] M. M. Islam, M. Shahruzzaman, S. Biswas, M. Nurus Sakib, and T. U. Rashid, "Chitosan based bioactive materials in tissue engineering applications-A review," *Bioact. Mater.*, vol. 5, no. 1, pp. 164–183, Mar. 2020.

[70] I. Hasa *et al.*, "Challenges of today for Na-based batteries of the future: From materials to cell metrics," *J. Power Sources*, vol. 482, p. 228872, Jan. 2021.

[71] T. Yuan *et al.*, "Novel Alkaline Zn/Na0.44MnO2 Dual-Ion Battery with a High Capacity and Long Cycle Lifespan," *ACS Appl. Mater. Interfaces*, vol. 10, no. 40, pp. 34108–34115, Oct. 2018.

[72] X. Jia, C. Liu, Z. G. Neale, J. Yang, and G. Cao, "Active Materials for Aqueous Zinc Ion Batteries: Synthesis, Crystal Structure, Morphology, and Electrochemistry," *Chem. Rev.*, vol. 120, no. 15, pp. 7795–7866, Aug. 2020.

[73] M. Li, "Preparation of composite materials for high-performance supercapacitors," L'UNIVERSITE DE LILLE, 2020. Accessed: May 06, 2022. [Online]. Available: https://tel.archives-ouvertes.fr/tel-03622572

[74] R. Zhang, "a Study of Flexible Supercapacitors: Design, Manufacture and Testing," *Coll. Eng. Des. Phys. Sci. Brunel Univ. London*, no. June, 2016.

[75] J. Yan, Q. Wang, T. Wei, and Z. Fan, "Recent Advances in Design and Fabrication of Electrochemical Supercapacitors with High Energy Densities," *Adv. Energy Mater.*, vol. 4, no. 4, p. 1300816, Mar. 2014.

[76] B. E. Conway and W. G. Pell, "Double-layer and pseudocapacitance types of electrochemical capacitors and their applications to the development of hybrid devices," *J. Solid State Electrochem.*, vol. 7, no. 9, pp. 637–644, Sep. 2003.

[77] G. G. Eshetu and E. Figgemeier, "Confronting the Challenges of Next-Generation Silicon Anode-Based Lithium-Ion Batteries: Role of Designer Electrolyte Additives and Polymeric Binders," *ChemSusChem*, vol. 12, no. 12, pp. 2515–2539, Jun. 2019.

[78] J. He and L. Zhang, "Polyvinyl alcohol grafted poly (acrylic acid) as water-soluble binder with enhanced adhesion capability and electrochemical performances for Si anode," *J. Alloys Compd.*, vol. 763, pp. 228–240, Sep. 2018.

[79] N. Lingappan, L. Kong, and M. Pecht, "The significance of aqueous binders in lithium-ion batteries," *Renew. Sustain. Energy Rev.*, vol. 147, p. 111227, Sep. 2021.

[80] H. K. Park, B. S. Kong, and E. S. Oh, "Effect of high adhesive polyvinyl alcohol binder on the anodes of lithium ion batteries," *Electrochem. commun.*, vol. 13, no. 10, pp. 1051–1053, Oct. 2011.

[81] M. Moniruzzaman, A. Akib, R. Shakil, S. Khatun, C. Kumar Roy, and A.-N. Chowdury, "Influence of Binder in the Fabrication of AC-Based High-Performance Electrochemical Supercapacitors," *ECS Trans.*, vol. 107, no. 1, pp. 18357–18365, Apr. 2022.

[82] J. Ji, F. Liu, N. A. Hashim, M. R. M. Abed, and K. Li, "Poly(vinylidene fluoride) (PVDF) membranes for fluid separation," *Reactive and Functional Polymers*, vol. 86. Elsevier, pp. 134–153, 2015.

[83] M. S. Rahman *et al.*, "Recent developments of carboxymethyl cellulose," *Polymers*, vol. 13, no. 8. MDPI AG, Apr. 2021.

[84] R. Gordon, R. Orias, and N. Willenbacher, "Effect of carboxymethyl cellulose on the flow behavior of lithium-ion battery anode slurries and the electrical as well as mechanical properties of corresponding dry layers," *J. Mater. Sci.*, vol. 55, no. 33, pp. 15867–15881, Nov. 2020.

[85] A. Tranchot, H. Idrissi, P. X. Thivel, and L. Roué, "Impact of the Slurry pH on the Expansion/Contraction Behavior of Silicon/Carbon/Carboxymethylcellulose Electrodes for Li-Ion Batteries," *J. Electrochem. Soc.*, vol. 163, no. 6, pp. A1020--A1026, Mar. 2016.

[86] D. Mazouzi *et al.*, "CMC-citric acid Cu(II) cross-linked binder approach to improve the electrochemical performance of Si-based electrodes," *Electrochim. Acta*, vol. 304, pp. 495–504, May 2019.

[87] J. Hu, Y. Wang, D. Li, and Y. T. Cheng, "Effects of adhesion and cohesion on the electrochemical performance and durability of silicon composite electrodes," *J. Power Sources*, vol. 397, pp. 223–230, Sep. 2018.

[88] M. G. A. Vieira, M. A. Da Silva, L. O. Dos Santos, and M. M. Beppu, "Natural-based plasticizers and biopolymer films: A review," *European Polymer Journal*, vol. 47, no. 3. Pergamon, pp. 254–263, Mar. 2011.

[89] X. Chen, N. Yao, B. S. Zeng, and Q. Zhang, "Ion–solvent chemistry in lithium battery electrolytes: From mono-solvent to multi-solvent complexes," *Fundam. Res.*, vol. 1, no. 4, pp. 393–398, Jul. 2021.

[90] S. Ahmed, A. Ahmed, and M. Rafat, "Supercapacitor performance of activated carbon derived from rotten carrot in aqueous, organic and ionic liquid based electrolytes," *J. Saudi Chem. Soc.*, vol. 22, no. 8, pp. 993–1002, Dec. 2018.

[91] M. Finšgar, K. Xhanari, and H. O. Ćurković, "Cyclic Voltammetry as an Electroanalytical Tool for Analysing the Reaction Mechanisms of Copper in Chloride Solution Containing Different Azole Compounds," *Curr. Anal. Chem.*, vol. 16, no. 4, pp. 465–474, Jul. 2018.

[92] D. Zhang, B. N. Popov, and R. E. White, "Modeling Lithium Intercalation of a Single Spinel Particle under Potentiodynamic Control," *J. Electrochem. Soc.*, vol. 147, no. 3, p. 831, Mar. 2000.

[93] P. Zhao, H. Zhang, H. Zhou, and B. Yi, "Nickel foam and carbon felt applications for sodium polysulfide/bromine redox flow battery electrodes," *Electrochim. Acta*, vol. 51, no. 6, pp. 1091–1098, Nov. 2005.

[94] S. M. Youssry, M. Abd Elkodous, G. Kawamura, and A. Matsuda, "Carbon dots conjugated nanocomposite for the enhanced electrochemical performance of supercapacitor electrodes," *RSC Adv.*, vol. 11, no. 63, pp. 39636–39645, Dec. 2021.

[95] R. M. Souto, M. M. Laz, and R. L. Reis, "Degradation characteristics of hydroxyapatite coatings on orthopaedic TiAlV in simulated physiological media investigated by electrochemical impedance spectroscopy," *Biomaterials*, vol. 24, no. 23, pp. 4213–4221, Oct. 2003.

[96] A. Lasia, "Electrochemical Impedance Spectroscopy and its Applications," in *Modern Aspects of Electrochemistry*, Kluwer Academic Publishers, pp. 143–248, 2005.

[97] N. Meddings *et al.*, "Application of electrochemical impedance spectroscopy to commercial Li-ion cells: A review," *Journal of Power Sources*, vol. 480. Elsevier B.V., p. 228742, Dec. 2020.

[98] M. Shimizu, H. Usui, and H. Sakaguchi, "Functional ionic liquids for enhancement of Li-ion transfer: the effect of cation structure on the charge–discharge performance of the $Li_4Ti_5O_{12}$ electrode," *Phys. Chem. Chem. Phys.*, vol. 18, no. 7, pp. 5139–5147, 2016.

[99] H. S. Magar, R. Y. A. Hassan, and A. Mulchandani, "Electrochemical Impedance Spectroscopy (EIS): Principles, Construction, and Biosensing Applications," *Sensors*, vol. 21, no. 19, p. 6578, Oct. 2021.

[100] M. Rychcik and M. Skyllas-Kazacos, "Evaluation of electrode materials for vanadium redox cell," *J. Power Sources*, vol. 19, no. 1, pp. 45–54, Jan. 1987.

CHAPTER-2

EXPERIMENTAL

2. EXPERIMENTAL

2.1 Chemicals

All of the chemicals and reagents utilized in this experiment were analytical grade, and they have been used without additional purification within the lab. The synthesis and washing of this work were done with double distilled water.
The following substances and reagents were used in this work:
Table 2. 1: The list of chemicals that were used in this work is given with the name of origin:

Name of the Chemicals	Source
Polyvinylidene Fluoride (PVDF)	Merck, Germany
Polyvinyl Alcohol (PVA)	Merck, Germany
Carboxymethyl Cellulose (CMC)	Merck, Germany
Hydrochloric Acid (HCl)	Sigma-Aldrich
Potassium Carbonate (K_2CO_3)	Sigma-Aldrich
Dimethyl Sulfoxide (DMSO)	RCI Labscan, Thailand
Sodium Sulfate (Na_2SO_4)	Sigma-Aldrich
Ethanol (C_2H_5OH)	Lab-Scan, Ireland
Sulfuric Acid (H_2SO_4)	Sigma-Aldrich, USA
Acetonitrile (C_2H_3N)	Merck, Germany
Tetraethylammonium Tetrafluoroborate ($C_8H_{20}BF_4N$)	Merck, Germany

2.2 Instruments

Instruments utilized in the sample synthesis as well as sample analysis included the following:

i. Electrochemical workstation (CHI 660 E, USA): is used for electrochemical measurement.
ii. Muffle furnace (Nabertherm, Germany, LT 5/12): to allow rapid high-temperature heating, recovery, and cooling in self-contained, energy-efficient cabinets.
iii. pH meter (LAQUA, F-74, HORIBA): to measure hydrogen-ion activity (acidity or alkalinity) in solution
iv. Centrifuge machine (Universal 16A, Hettich, Germany): to separate various components of a fluid.
v. Hotplate and Digital stirrer (Snidjers, 34532): is used for mixing and heating aqueous solutions **for** a great variety of chemical reactions.

vi. Drying oven (Lab Tech, LDO-030E): to maintain a consistent, uniform temperature for the solid materials being investigated in the natural environment.

vii. Vacuum oven (HYSC, VO-27):is used for drying heat-sensitive materials such as powder to extract moisture at a low temperature.

viii. Ultrasonicator (Powersonic 603, Korea): to make sure that all the components in a liquid system get mixed together as much as possible.

ix. Digital Balance (D99-09-030 Precisa Gravimetrics AG): to get the sample's exact mass (quantity).

x. Field Emission Scanning Electron Microscopy (FE-SEM) (JEOL JSM-7600F, Tokyo, Japan):to obtain information about the surface topography and composition.

xi. Energy Dispersive X-ray Spectrophotometer (EDX, Oxford instruments, UK): to facilitate the elemental analysis or chemical characterization of a sample.

xii. Fourier Transform Infrared Spectrophotometer (FTIR-8400, Shimadzu, Japan): to investigate the function groups of the examined matrices

2.3 Synthesis of Activated carbon (AC)

Banana leaves as the precursor material was collected from the BUET residential area in Dhaka, Bangladesh. A chemical activation procedure was used to prepare the activated carbon from this precursor material. Specifically, banana leaves were gathered, sliced into tiny pieces, and washed with deionized water (DI).The banana leaves were then dried for 24 hours at 85°C in an oven to eliminate moisture.For impregnation, K_2CO_3 is combined with the precursor and utilized as an activating agent in a 1:2 ratio, as shown in equation 1.

$$\text{Impregnation Ratio (IR)} = \frac{\text{Mass of Activation Agent (g)}}{\text{Mass of CDS (g)}} \quad \text{.....(1)}$$

In the following, the carbonization process was operated at 750 °C for 5 hours at a rate of 10 min^{-1} in an N_2 environment.After cooling, the resultant mixture was steeped in 1 M HCl and then repeatedly rinsed with DI water until the P^H reached neutral.Finally, the samples were dried in an

electric oven at 80 °C for 12 hours to attain the proper surface area of activated carbon.The preparation technique is shown schematically in Figure 2.

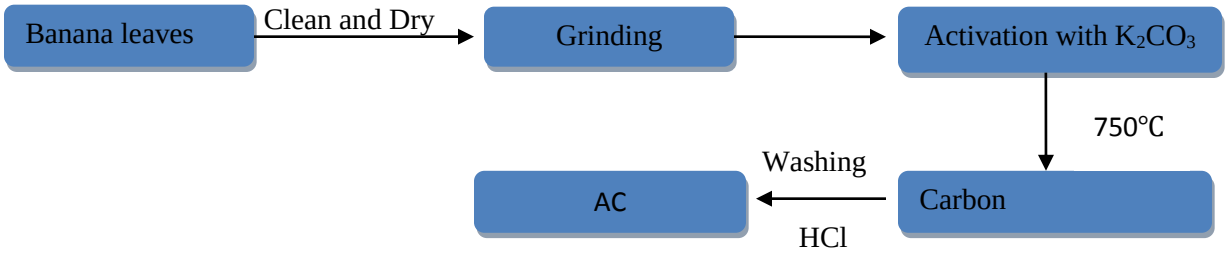

Scheme 2. 1: Schematic illustration of the process of fabricating activated carbon from banana leaves.

2.4 Fabrication of AC-Modified Graphite (ACGM) Electrodes

The most cost-effective electrode for manufacturing using our synthesized materials was a graphite rod (diameter: 6.13 mm, length: 8.00 cm) acquired from Otool World, USA. A shrinkable polymeric tube was used to secure the rod to a disk electrode. In an electrochemical setup, this manufactured graphite electrode serves as the working electrode.Samples were collected in a vial with a binder to build a modified graphite electrode. By sonication, the mixtures (sample plus binder) were fully disseminated in DMSO.A 20μL -dispersed solution was deposited on the polished surface of the naked graphite electrode.The manufactured electrode was dried in an oven overnight at 65 ℃.Scheme 2.2 depicts the graphite electrode production process.

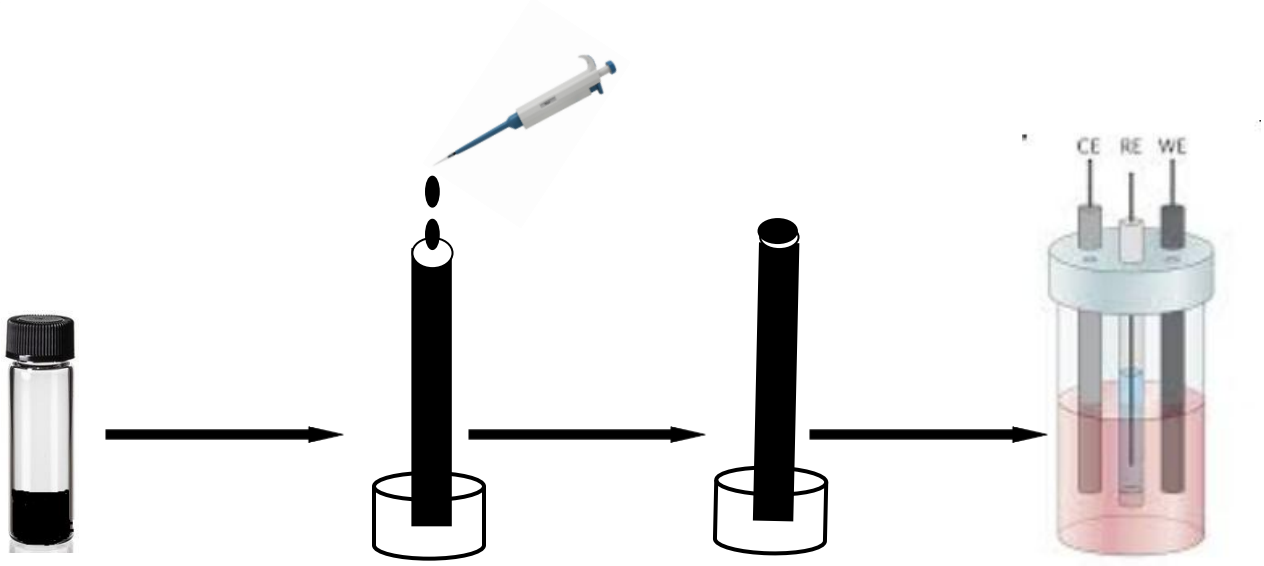

Solution Electrode | Bare Graphite Electrode | Modified Graphite Set Up | Electrochemical

Scheme 2. 2: Fabrication of graphite electrode for electrochemical measurements

2.5 Swelling Test

Swell tests on the expanding binder were performed to detect changes in swelling potential. The experimental program in this study was performed according to Komaba's report.The swelling properties of the as-obtained electrodes in different binder systems are inspected by soaking them in the electrolyte solution at ambient temperature for 48 h, in order to account for the good electrochemical stability.

The swelling ratios were calculated using the formula below:

$$\text{Swelling \%} = \frac{\text{Weight (s)} \times \text{Weight (dry)}}{\text{Weight (s)}} \times 100\%$$

2.6 Thermal Diffusivity Test

Thermal diffusivity (in mm2/s) is a material-specific characteristic used to describe uneven heat conduction. This number indicates how rapidly a material responds to temperature changes. Thermal diffusivity must be known in order to predict how cooling will work or to model temperature fields. It is also necessary to solve the Fourier differential equation for unsteady heat conduction. Moreover, thermal diffusivity is related to supercapacitor safety and has a substantial influence on supercapacitor safety performance. Thermal diffusivity is denoted by the letter D or α (alpha).SI unit of thermal diffusivity is m^2/s.

2.7 Characterization

2.7.1 FT-IR Spectroscopy

Fourier Transform Infrared Spectrometry (FTIR) is one of the most popular and widely used spectroscopic techniques for detecting the infrared spectrum of absorption, emission, and photoconductivity of solids, liquids, and gases. It's necessary for obtaining specific information on the functional groups in the materials. It's a graph of measured intensity vs. IR wave number for a solid, liquid, or gas sample, and it's based on molecules' unique infrared light absorption (IR). FT-IR spectra may be seen between 4000 and 400 cm^{-1}. The incident beam is split into two beams in modern dispersive spectrometers, one of which passes through the sample and the other via a suitable reference material. An appropriate detector monitors the strength of both beams, and the final data output may be shown in either transmittance or absorbance. The final plot is a graphical depiction of transmittance or absorbance with a wavelength or frequency, known as the spectrum, which happens at each wavelength element. A KBr pellet was used to conduct the FT-IR analysis of the sample. The sample to KBr weight ratio was roughly 1:200. The instrument's picture image is displayed in Fig. 2.3.

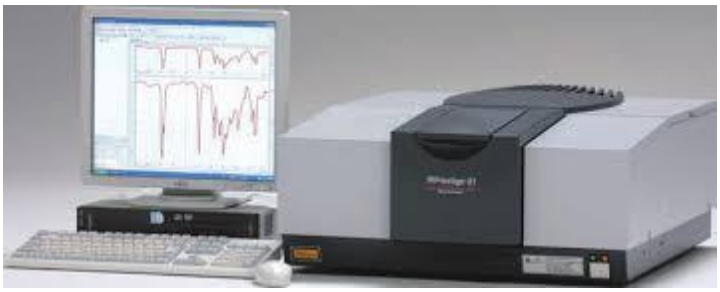

Figure 2. 1: Digital image of the Shimadzu-FTIR-8400 FTIR equipment.

In order to produce spectrum in our experiments, the synthesized components were employed to manufacture pellets containing KBr. The vibration spectra of the samples were recorded using a Perkin Elmer FT-IR spectrophotometer. 200 mg of KBr and 1-2 mg of materials were combined, homogeneously crushed, and pressed to produce a pellet. Background correction was performed using a pure KBr pellet to eliminate the contribution of infrared-active ambient gases such as carbon dioxide and water vapor in the sample spectra.

2.7.2 Scanning Electron Microscopy (SEM)

SEM is sophisticated equipment that scans the surface of a sample with a focused beam of electrons to obtain pictures of the material. When electrons contact atoms in a sample, data about the sample's surface topography and composition is produced. The electron cannot produce and accelerate electrons; an electromagnetic lens focuses the electrons, a vacuum chamber houses the specimen stage, and a detector collects the signals generated by the specimen in a scanning electron microscope. Fig. 2.3 shows the image of the JSM-7600F (FE-SEM, Tokyo, Japan) equipment.

Figure 2. 2: Scanning Electron Microscopy (SEM) setup at Department of Glass and Ceramic Engineering (GCE), BUET.

To investigate the morphology of produced composites, we used scanning electron microscopy (JSM-7600F, Japan). The electron cannon had a probe current of 1.0 nA and a 20 kV acceleration voltage. The perimeter, circularity, solidity, and quantity of nano-sized particles in SEM images of composites at a specific scale were measured using computer-adapted software (ImageJ 64-bit Java 1.8.0 112).

2.8 Electrochemical Measurements

2.8.1 Electrochemical Analyzer with Cell and Electrodes

A computer-controlled electrochemical analyzer was used for all electrochemical measurements. The schematic arrangement of the computerized electrochemical analyzer system's instrumental setup is shown in Figure 2.4.

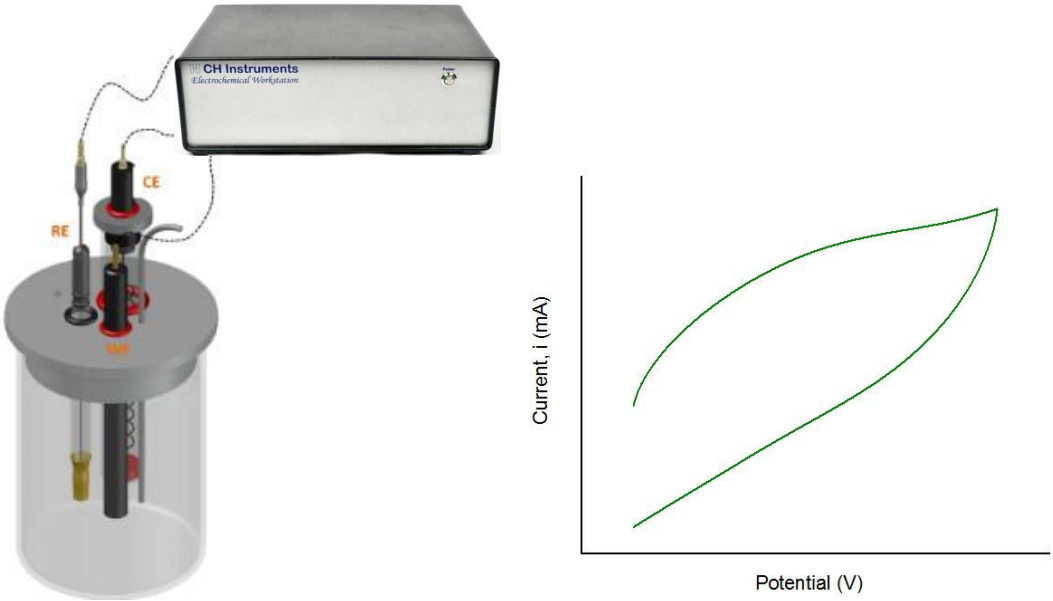

(a) (b)

Figure 2. 3: (a) Electrochemical setup, and (b) schematic CV

Electrochemical experiments were carried out in a single compartment with three electrodes. In our electrochemical studies, We employed a graphite electrode from a local market as the working electrode, platinum (Pt) wire as the counter electrode, and silver-silver chloride [Ag/AgCl|KCl (saturated in water)] as the reference electrode. The reference electrode's purpose is to serve as a reference point for monitoring and adjusting the working electrode potential. All electrochemical studies for a single sample, such as cyclic voltammetry, chronopotentiometry, and electrochemical impedance measurements, were done simultaneously, one after the other, using the same setup.

2.8.2 Performance Evaluation of the Modified Graphite Electrodes

a. Cyclic Voltammetric Measurements

The cyclic voltammetric experiments aimed to select the perfect potential window when no oxidation-reeducation happens. Selecting a non-faradic potential zone for pure EDLCs is thus critical. The possible windows for EDLCs vary depending on the electrolyte. For example, we measured the CVs of modified graphite AC electrodes in an aqueous 0.5 M Na_2S0_4 solution between -0.7 and +0.7 V. All adjusted electrode CVs were then collected within this set potential range.

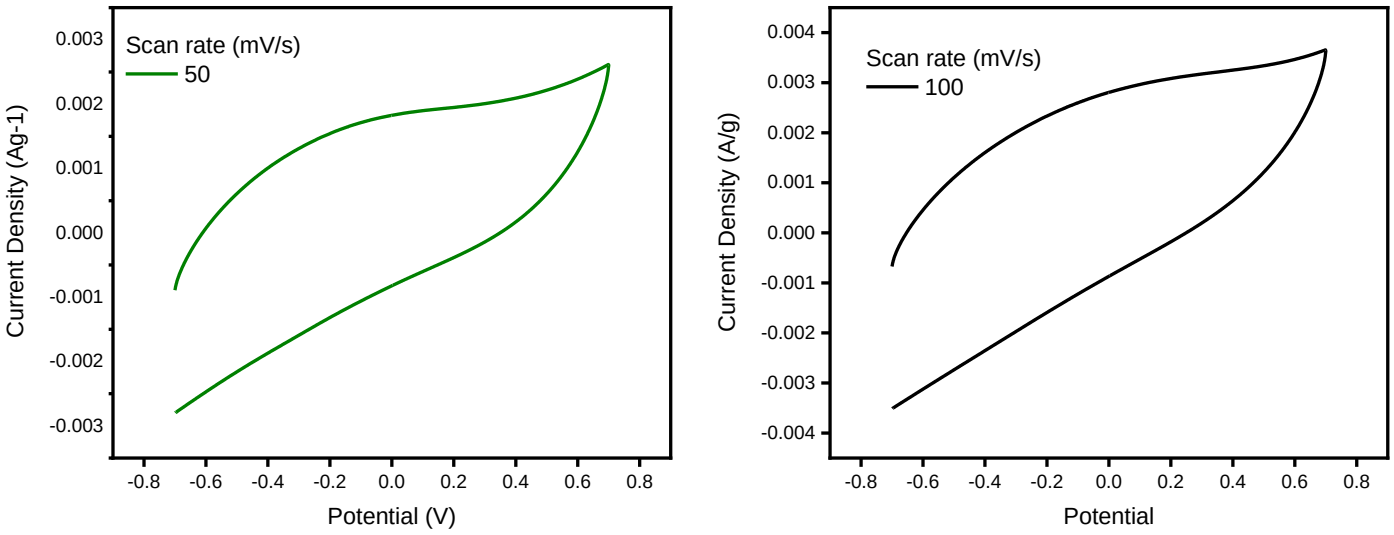

Figure 2. 4: Typical CVs of AC-based modified graphite electrode within two different potential windows in 0.5 M Na_2SO_4 solution.

In the CV experiment, an immersed, stationary electrode is scanned from a beginning potential to a final potential, which is known as the switching potential. After then, a reverse scan is done to ensure that the potential range remains the same. This produces a "cyclic" sweep of potentials that I may repeat as needed. The cyclic voltammogram (CV) curve is defined by the current vs. potential curve. The d-ata was used to create the curve. The "scan window" refers to the probable extreme endpoints. The first sweep is known as the "forward scan," while the second is known as the "reverse scan."One of the most remarkable features of CV is that the total current increases as the scan rate increases. The scan rate is defined as the rate at which potential changes over time. The size of the diffusion layer, as well as the time it took to record the scan, may both be utilized to justify the situation.The primary characteristics are the type of the analyte, its concentration, the scan speeds, and the experimental circumstances. The size of the current response and the form of the voltage voltammograms can both be affected by this. Cyclic voltammetry can provide information about the dependence of the stability of the complex transition

metal oxidation state, the reversibility of electron transfer processes, the reactivity of active materials, and so on by modifying these parameters.

b. Chronopotentiommetric Measurements

Chronopotentiommetric measurements were carried out to calculate C_{sp} from the charge-discharge curves as well as to find the cycle stability. The chronopotentiometry of prepared electrodes were carried out in different solution varying current density from 1 to 3 Ag^{-1} within a suitable potential window which was chosen from CV. Following equation is used to calculate C_{sp} of our materials.

$$C_{sp} = \frac{i\,\Delta t}{m\Delta V} \qquad (1)$$

Where, C_{sp} is the specific capacitance, I is discharge current (cathodic current), m is the mass of active electrode material, Δt is the total time of discharge and ΔV is t he potential drop during discharge. The specific power density (P_s) and specific energy density (E_s) were calculated from the chronopotentiograms usingthe following equations:

$$E = 0.5 \times Csp(\Delta V)^2/3.6 \qquad (2)$$

$$P = E \times 3600/\Delta t \qquad (3)$$

Cycle stability is tested within same potential window as for CV of the prepared composites by observing C_s for 5000 cycles at higher current density 10 Ag^{-1} in 0.5 M Na_2S0_4 solution. Also columbic efficiency can contribute to calculate the cycle stability of electrode materials. Coulombic efficiency of supercapacitor is defined as the ratio of discharging time and charging time as follows-

$$\eta = \frac{t_d}{t_c} \times 100\ \% \qquad (4)$$

Where, η is the columbic efficiency, t_d the discharging time (s), and t_c is charging time (s)

2.8.3 Electrochemical Impedance Spectroscopy Measurement

EIS measurements of our created samples were performed because of their ability to distinguish the contributions of various components of the investigated electrochemical system. To investigate mechanistic information and reactions occurring at the electrode surface, data from EIS was used to create an equivalent electrical circuit with circuit elements such as series resistance (Rs), electrochemical double-layer capacitor (CdI), charge transfer capacitance (Rct),

pore resistance (Rp), pore capacitance (Cp), Warburg element (Zw), and constant phase element (CPE).

The CHI 660E (USA) electrochemical analyzer was used to conduct EIS measurements at various AC potentials of the working electrode. In the frequency range of 100 kHz to 0.1 Hz, impedance data was acquired. The CHI 660 E software was used for the modeling of experimental data.

2.9 References

[1] Ogungbenro. A. E., Quang. D. V., Al-Ali. K. A., Vega. L. F. and Abu-Zahra. M. R. M., "Synthesis and characterization of activated carbon from biomass date seeds for carbon dioxide adsorption," *J. Environ. Chem. Eng.*, vol. 8, no. 5, p. 104257, Oct. 2020.

[2] Roy. C. K *et al.*, "Preparation of Hierarchical Porous Activated Carbon from Banana Leaves for High-performance Supercapacitor: Effect of Type of Electrolytes on Performance," *Chem. – Asian J.*, vol. 16, no. 4, pp. 296–308, Feb. 2021.

[3] Egerton. R. F., *Physical Principles of Electron Microscopy*. Boston, MA: Springer US, 2005.

[4] Goldstein. J. I., Joy. D. C., Michael. J. R., Newbury. D. E., Ritchie. N. W. M., and Scott. J. H. J., *Scanning Electron Microscopy and X-Ray Microanalysis*, 4th ed. 2018. New York, NY: Springer New York : Imprint: Springer, 2018.

[6] Toigo. C., Singh. M., Gmeiner. B., Biso. M., and Pettinger. K.-H., "A Method to Measure the Swelling of Water-Soluble PVDF Binder System and Its Electrochemical Performance for Lithium Ion Batteries," *J. Electrochem. Soc.*, vol. 167, no. 2, p. 020514, Jan. 2020.

[6] Potenza. M., Coppa. P., Corasaniti. S., and Bovesecchi. G., "Numerical Simulation of Thermal Diffusivity Measurements With the Laser-Flash Method to Evaluate the Effective Property of Composite Materials," *J. Heat Transf.*, vol. 143, no. 7, p. 072102, Jul. 2021.

[7] Zhang. J*et al.*, "Application of Fourier transform infrared spectroscopy with chemometrics on postmortem interval estimation based on pericardial fluids," *Sci. Rep.*, vol. 7, no. 1, p. 18013, Dec. 2017.

CHAPTER-3

RESULTS AND DISCUSSION

3.1Structure, Morphology and Elemental analysis

3.1.1: Structure and Surface Morphology Analysis

Scanning electron microscopy (SEM) is a kind of imaging that utilizes electrons. The incoming electron beam is swept over the sample's surface in a raster pattern and backscattered or secondary electrons are detected [1]. A field emitter (FE-SEM) is a cathode that emits electrons under the influence of a very strong electric field, resulting in better pictures. Although sample preparation is straightforward, the electron beam might cause biological material to degrade, therefore it should only be used for small samples. Environmental or wet SEM is a recent technology that does not need sample drying and keeps the topography of the sample. The synthesized ACNSs, CMC, PVA, PVDF were analyzed by SEM image given in Fig.

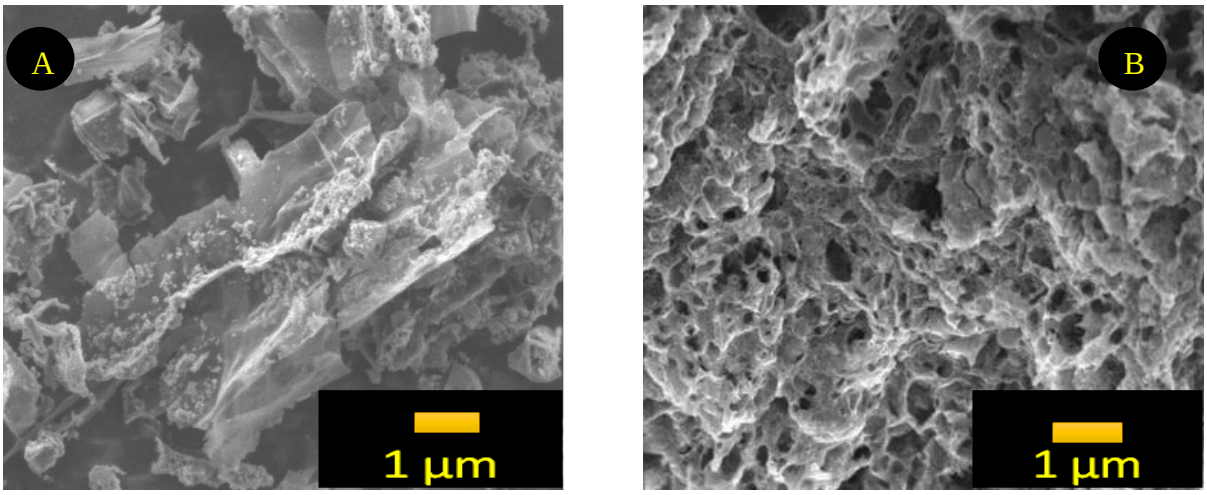

Figure 3. 1: SEM images of activated carbon (a) before and (b) after the activation process

Figure 3.1 (B) shows the FESEM of AC. As can be observed in the FESEM image, it provides the clear evidence of the change in surface morphology of the carbon materials. Before activation, carbon material has stack layer formation with very nominal level hierarchical porous structure. But after adsorption it becomes semi crystalline with a huge number of pores. That means, it surfaces area are increased, which is an important criterion for enhancing the electrochemical performance [2].

C. SEM Image of AC-CMC

The surface morphology and particle size were determined using FESEM analysis. The SEM images of AC-CMC are shown in Figure 3.2. The images demonstrate that the resultant image gel or sponge-like formation has a non-uniform pore size and an irregular shape, which is one of the features of amorphous.

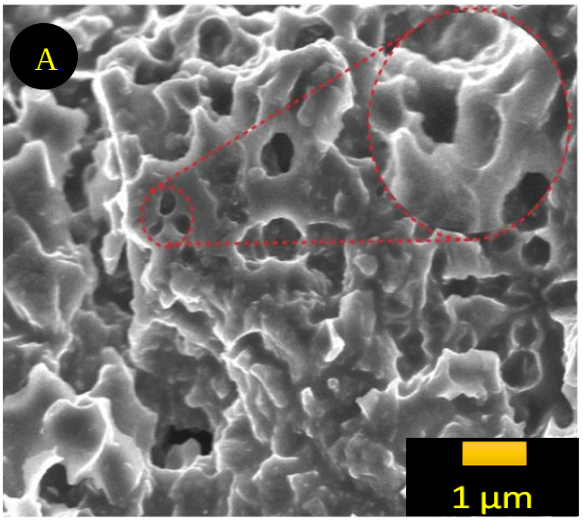

Figure 3. 2: SEM images of AC-CMC

b. SEM Image of AC-PVDF

The phase morphology of AC-PVDF was investigated using SEM. It can be noticed in Figure 3.3, AC-PVDF particles shows nearly appears Spherical particles, gather together like roe, but they are not all the same size and shape, and the differential particle size histogram size ranges from 20 nm to 40 nm.

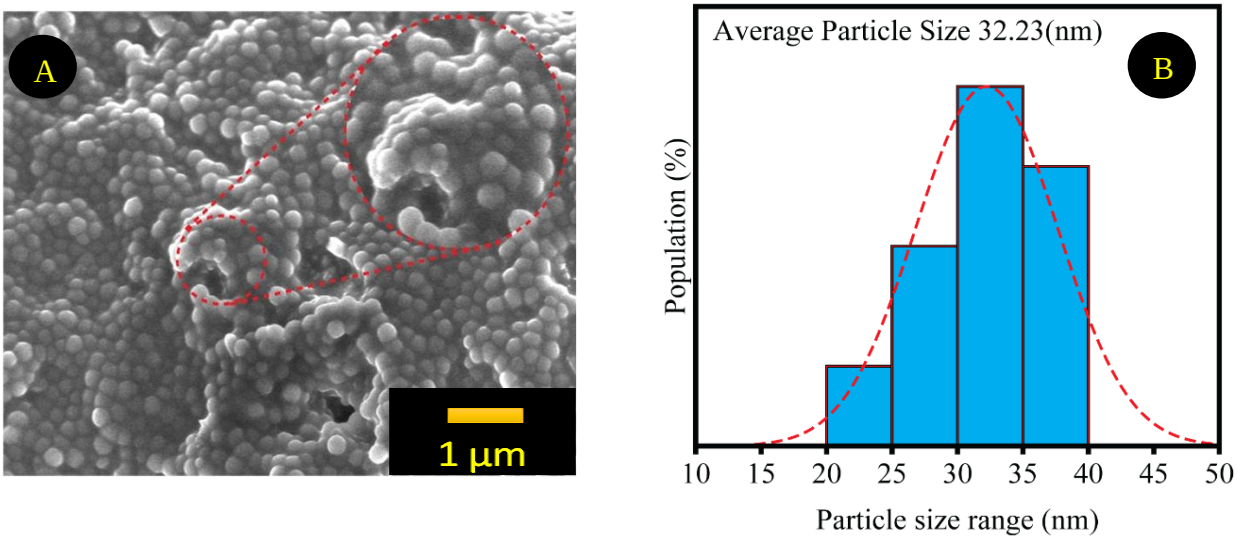

Figure 3. 3: (a) SEM images of AC-PVDF and (b) Particle size distribution analysis of AC-PVDF by SEM

C. SEM Image of AC-PVA

To observe the particle size and internal microstructure of AC-PVA, SEM tests were performed. Figure 3.4 displays 10000x magnification SEM images. It can be clearly noticed that the resulting particles are nano-sized and have a well-defined morphology. The particle sizes are not identical, and the particle size distribution is depicted in figure 3.4(B). The average particle size was reported to be in the 482.47 nm range.

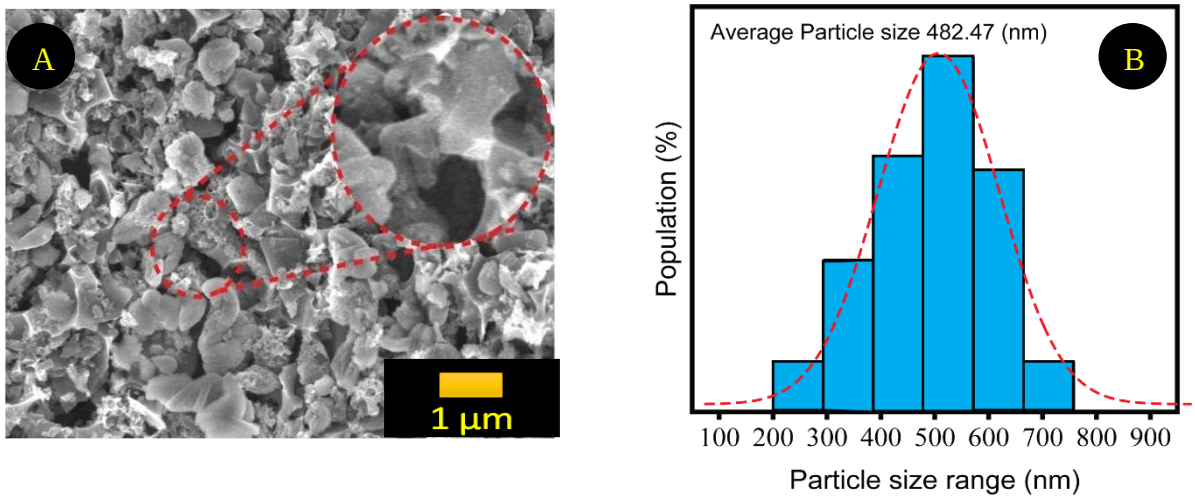

Figure 3. 4: (a) SEM images of AC-PVA and (b) Particle size distribution analysis of AC-PVA by SEM

3.1.2 Elemental Analysis

a. EDS Analysis of AC

EDS spectra of the samples were used to figure out the chemical compositions of AC [3]. During EDS studies, different areas were addressed, and the correlating peaks are presented in Figure 3.5.The EDS analysis of the activated carbon revealed that it had 93.16% carbon, 2.54% oxygen, and 2.65% silicon, indicating the presence of the three essential components (carbon, oxygen, and silicon). Additionally, the EDS analysis also reveals no potassium (K) in the activated carbon. This is a result of the activated carbon being thoroughly washed with hydrochloric acid (HCl), which eliminates all residues of potassium. The elements' atomic weight percentages are listed in detail in Table 3.1.

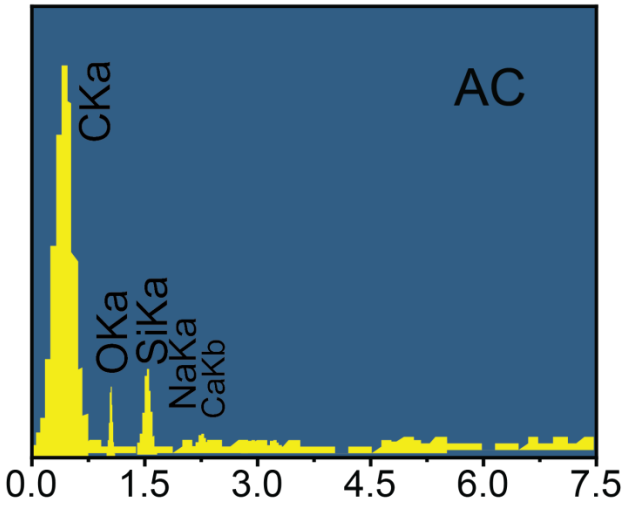

Figure 3. 5: Elemental analysis of as-synthesized AC

Table 3. 1: contains a detailed representation of the atomic weight percentages of the elements

Samples	Atomic Percentage of elements in the samples		
AC	C	O	Si
	93.16	2.54	2.65

b. EDS Analysis of AC-CMC

Elemental analysis of the AC-CMC was achieved from the EDS spectra as presented in Figure 3.6 [4]. The C peak was observed at 0.277 keV and 0.525 keV for K lines of the oxyzen element. In addition to these peaks, the presence of the peak of 1.041 KeV corresponding to the Na element According to the EDS spectrum, the average quantities of C, O, and Na in the prepared AC-CMC are 92.82 % , 6.59 %, and 0.24%, respectively. So, the EDX data confirms the presence of required elements in synthesized nanocomposites. In Table 3.2, the atomic weight percentages of the elements are presented in detail.

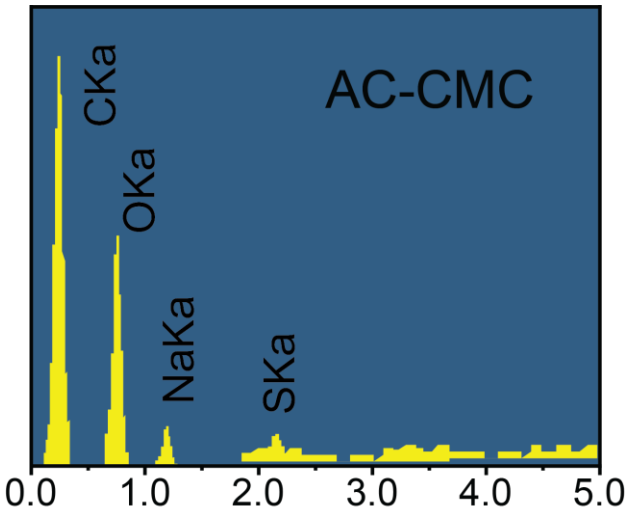

Figure 3. 6: Elemental analysis of as-synthesized AC-CMC

Table 3. 2: contains a detailed representation of the atomic weight percentages of the elements

Samples	Atomic Percentage of elements in the samples		
AC	C	O	Na
	92.82	6.59	0.24

c. EDS Analysis of AC-PVDF

The elements present in the AC-PVDF composite were exploited by EDS analysis [5]. Figure 3.7 shows the EDS spectrum of AC-PVDF where C, O, and F elements show their characteristic peaks. The average quantities of C, O and F in the prepared AC-PVDF are 74.78%, 15.33% and 9.38 % respectively. Therefore, the EDX data indicates the existence of needed components in nanocomposites that have been synthesized.Presence of different elements as their corresponding atomic% is shown in Table 3.3.

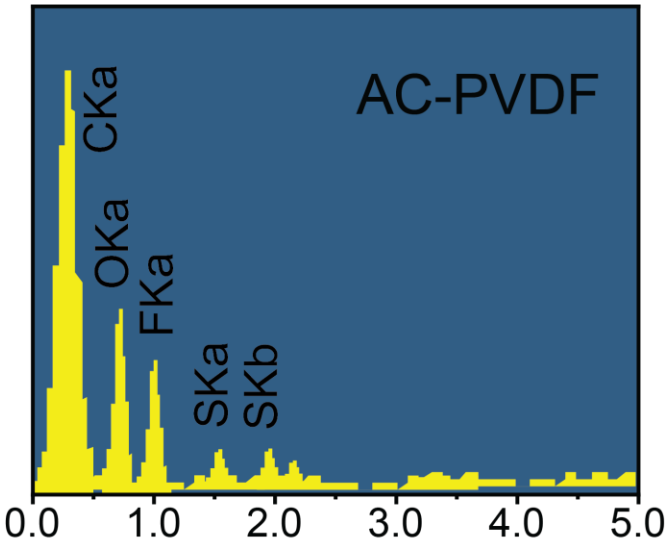

Figure 3. 7: Elemental analysis of as-synthesized AC-PVDF

Table 3. 3: Elemental composition of AC-PVDF composite

Samples	Atomic Percentage of elements in the samples		
AC	C	O	F
	74.78	15.33	9.38

d. EDS Analysis of AC-PVA

The elemental analysis of the AC-PVA was performed using EDS equipment on the SEM as shown in Figure 3.8 [6]. The C peak was observed at 0.277 keV and 0.525 keV for k lines of the oxygen element. The peak of 2.307 keV corresponds to the S element. According to the EDS spectrum, the average quantities of C, O, and S in the prepared AC-PVA are 65.82%,

33.73%, and 0.46%, respectively. Table 3.4 shows the presence of various elements as a percentage of their total atomic weight.

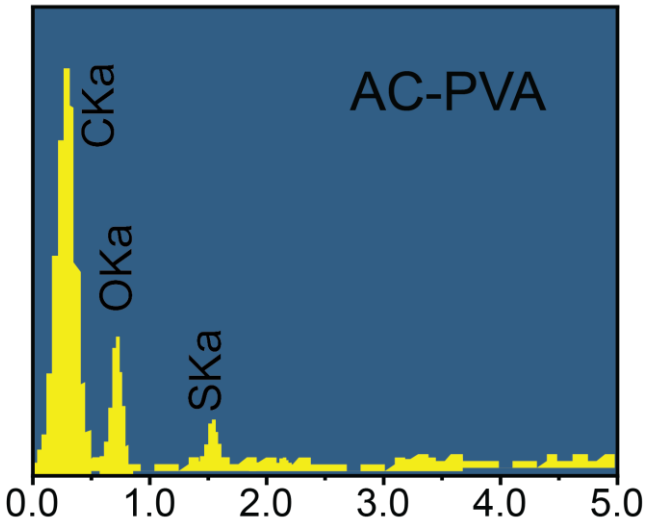

Figure 3. 8: EDS spectra of AC-PVA

Table 3. 4: Elemental composition of AC-PVA composite

Samples	Atomic Percentage of elements in the samples		
AC	C	O	s
	65.82	33.73	0.45

Thus, the chemical composition obtained from the EDX spectrum, it can be calculated that the composition of the prepared sample is AC-PVA and no foreign element were present.

3.1.3 Functional Group Analysis

FT-IR spectral analysis provides some useful qualitative information on the identification of compounds. Both organic and inorganic substrates absorb IR light and thus IR active. The frequency range is measured as wave numbers over range (400-4000 cm^{-1}). The characteristic peaks for different functional groups of these species in FT-IR spectra with peaks assignment are presented in Fig 3.9, 3.10 and 3.11.

a) FT-IR Analysis of AC-CMC

FTIR was employed to investigate the chemical composition of membranes.The FTIR spectrum of NCC was depicted in Fig. 3.9. As could be seen from Fig-3.9, the FTIR absorptions at 3340, 2901, 1430 and 1059 cm^{-1} were related to O–H stretching vibrations of CMC, C–H stretching vibrations of CMC, CH_2 scissor bending vibration, and C–O stretching vibrations of CMC, respectively [7]. The peak at 1072cm^{-1} represented stretching vibration of C–O–C that joins glucose units in the molecule of cellulose. Besides, the absorption at 1719, and 1632 cm^{-1}were attributed to bending vibration of absorbing of C=O and H–O–H groups respectively.

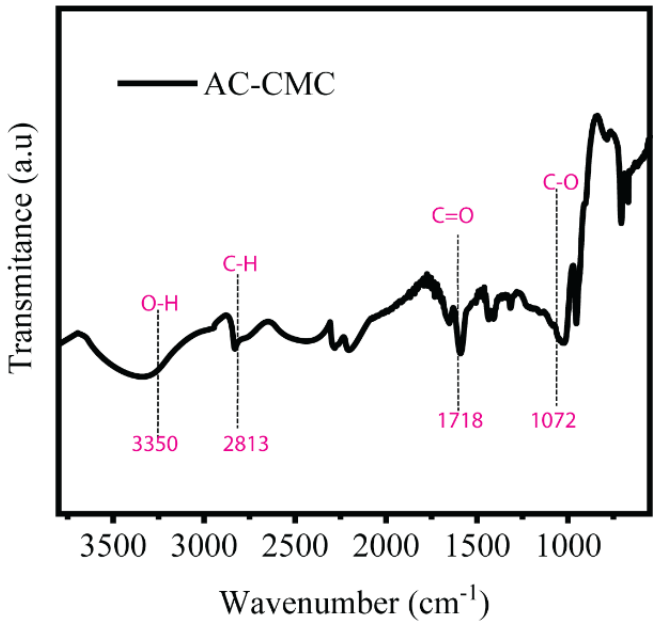

Figure 3. 9: FT-IR spectrum of AC-CMC

b) FT-IR Analysis of AC-PVDF

The FTIR spectra of the PVDF Composite binder were depicted in Fig 3.10. The bands located at 3022 and 2980 cm^{-1}corresponded to the CH_2 asymmetric and symmetric vibration of PVDF. The absorption peak appeared at 1403 cm^{-1} was attributed to CH_2 wagging vibration. The C–C band of PVDF was observed at 1185 cm^{-1}.The peaks at 878 and 840 cm^{-1} were related to C–C–C

asymmetrical stretching vibration and CF stretching vibration of PVDF [8-9]. It was observed that the characteristic absorption peaks of the pure PVDF membranes were retained by the spectrum of PVDF binder. For instance, the peaks at 3022 and 2980 cm^{-1}were related to the CH_2 asymmetric and symmetric vibration of PVDF. The peak at 1403 cm1 represented CH_2 wagging vibration was displayed. The peak at 840 cm^{-1} corresponded to C–F stretching vibration of PVDF was also observed in Fig. 3.10.

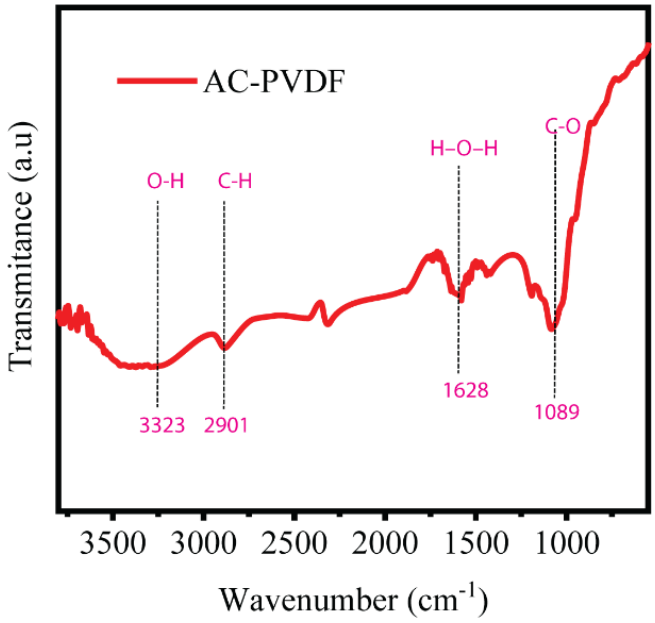

Figure 3. 10: FT-IR spectrum of AC-PVDF

C) FT-IR Analysis of AC-PVA

Generally, the vibrational spectra of PVA exhibit the characteristics of the vinyl alcohol monomer and it is expected to reveal 17 modes of vibrations [10]. The C–H wagging mode is expected to appear at about 1240 $cm^{-1}$for PVA. In this experiment, the C–H wagging mode appeared only after the acetylation process, which can be explained by a structural deformation of the PVA backbone. Another expected vibrational mode for PVA is the vibration mode of carbonyl stretching at about 1690 cm^{-1}. The carbonyl stretching vibration was observed at 1690 cm^{-1}PVA. Despite the acetylation of PVA moieties, the chain structure of PVA is, in general, breaking upon increasing the dose due to the bond scission because of the high energy of irradiation [11].

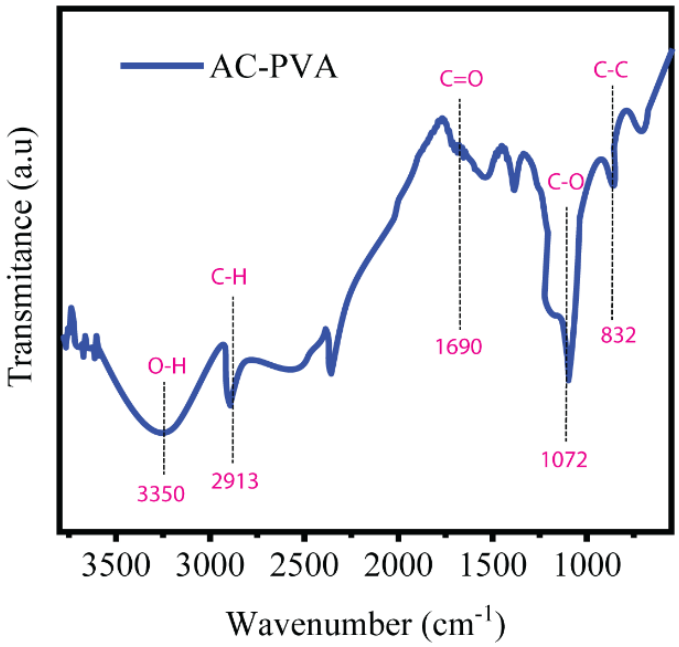

Figure 3. 11: FT-IR spectrum of AC-PVA

3.2 Swelling Test Analysis

Considering the swelling of binders is also an important factor for reversible stable cycling [12]. The swelling properties of the as-obtained electrodes in different binder systems are inspected by soaking them in the 0.5M sodium sulfate electrolyte solution at ambient temperature for 48 h, in order to account for the good electrochemical stability of the AC-PVA electrode. After cleaning the leftover electrolyte from the electrode surface in the glove box, the electrodes are removed to weight the mass. The starting weight of the electrodes is therefore specified as m_0. The increased mass percent $[(m_1-m_0)/ m_0]\times100\%$ of the electrode films in various binder systems are summarized in Table 3.5.Under the lab conditions, the weight increase of the electrode films due to the sulfate electrolyte absorption is 8.81 %, 7.97 %, and 4.41 % of the starting weight for electrodes with PVDF, CMC, and PVA binders, respectively. Furthermore, another essential experiment demonstrating the swelling feature is complemented by immediately soaking the binder granules in the electrolyte solution. Fig. 3.12 depicts the dissolving status before and after soaking. PVDF particles, as expected, swell, generating a viscous, gel-like fluid solution, which is consistent with previous research. PVA and CMC powders, on the other hand, do not swell under the same testing conditions. In brief, PVDF may readily expand by absorbing electrolyte solutions, resulting in electrolyte penetration into the whole composite electrode.

Table 3. 5: Swelling properties of the graphite electrode in three binder systems

Electrode (S)	Swelling property (%)
PVDF	**8.81**
CMC	**7.97**
PVA	**4.41**

Finally, excessive electrolyte penetration may loosen or destroy the electrically conductive network and active material in the PVDF composite electrode, resulting in capacity degradation and cycle life shortening after long-term cycling [13]. When compared to the PVDF system, the polymer can effectively suppress excessive electrolyte penetration and improve electrode integrity during cycles for PVA and CMC binder composite electrodes. PVDF powders, on the other hand, readily swell, forming a viscous, gel-like fluid product, which is consistent with other reports.

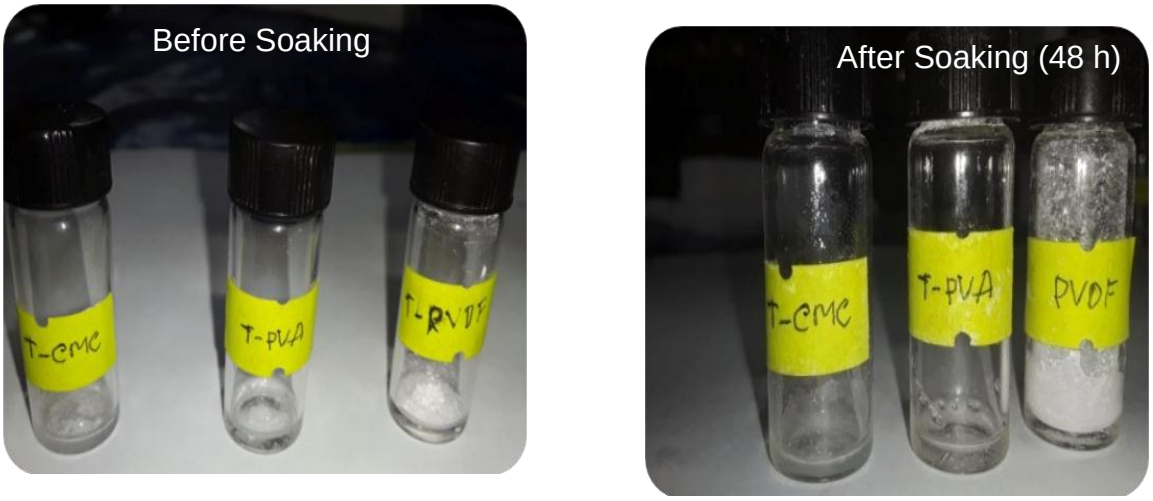

Figure 3. 12: The difference in the swelling of the binder powders in addition of the electrolyte solution

In contrast, PVA and CMC do not swell under the same experimental condition. Binder swelling must also be an important element in reversible cycling. PVDF may be swollen by absorbing electrolyte, resulting in electrolyte solution penetration throughout the whole composite electrode and electrode particle desquamation. According to Komaba's study, excessive electrolyte penetration may loosen or break the electrically conducting network in the PVDF composite electrode, resulting in capacity fading and cycle life shortening over a lengthy period of cycling. The polymer in the PVA binder composite electrode efficiently inhibits excessive electrolyte penetration and increases cycle performance when compared to the PVDF system.

3.3 Thermal Diffusivity Test

The term "thermal diffusivity" refers to the rate of the ability of a material to conduct temperature. Moreover, thermal diffusivity is related to supercapacitor safety and has a substantial influence on supercapacitor safety performance [15]. When a capacior experiences a sudden burst of high temperature, the PVA binder with the higher thermal diffusivity may swiftly dissipate the heat to the outside. The capacitor's external sensor may respond quickly. As a consequence, the chances of danger are minimized.

Table 3.6 shows the thermal diffusivity values of three polymeric binders to those published in the literature [16-17]. The PVA binder has the highest thermal diffusivity, almost three times that of CMC (1.0×10^{-7} m^2 s^{-1}) and PVDF ($0.6\times10^{-7}m^2s^{-1}$). This indicates the PVA binder has the maximum thermal diffusivity, indicating that AC-PVA is more secure for supercapacitor safety.

Binder	Thermal Diffusivity ($m^2 s^{-1}$)
PVA	**2.2×10^{-7}**
CMC	**1.0×10^{-7}**
PVDF	**0.6×10^{-7}**

Table 3. 6: Thermal diffusivity of the three polymeric binders

3.4 Investigation of Electrochemical Performance of AC-Modified Graphite (ACMG) Electrode with Different Polymeric Binders

The electrochemical measurements were studied in an electrochemical setup containing a working electrode, reference electrode and counter electrode for a modified graphite electrode. To study the electrochemical behavior of the modified electrode, researchers used three techniques: cyclic voltammetry, galvanostatic charge-discharge, and electrochemical impedance spectroscopy. Electrochemical setup, electrode modification, and electrochemical methods were all part of the experiment.

3.4.1 CV and GCD of ACMG in CMC Binder

CV and Corresponding GCD curves of AC modified graphite electrode in CMC are demonstrated in Figure 3.13. From these responses, C_s, determined is summarized in Table 3.7. Figure 3.13(a) represents the CV curves of AC-CMC modified graphite electrode in non-Faradic region for different scan rates. Here, electrochemical measurements were carried out in 0.5 M Na_2SO_4 Solution. CV's rectangular form allows for low contact resistance even at higher scan rates, implying that these systems exhibit desirable fast charge-discharge rates [18].It is observed that the CV of AC-CMC modified graphite electrodes has no oxidation and reduction peaks, which indicates the pure double-layer capacitance of our systems. However, the shapes of CVs are rectangular mirror images in size, and they slightly deform with increasing scan rates. The rectangular shape is slightly deformed with scan rates because the electrolyte ions get little time to penetrate the surface of the electrode at a high scan rate [19].

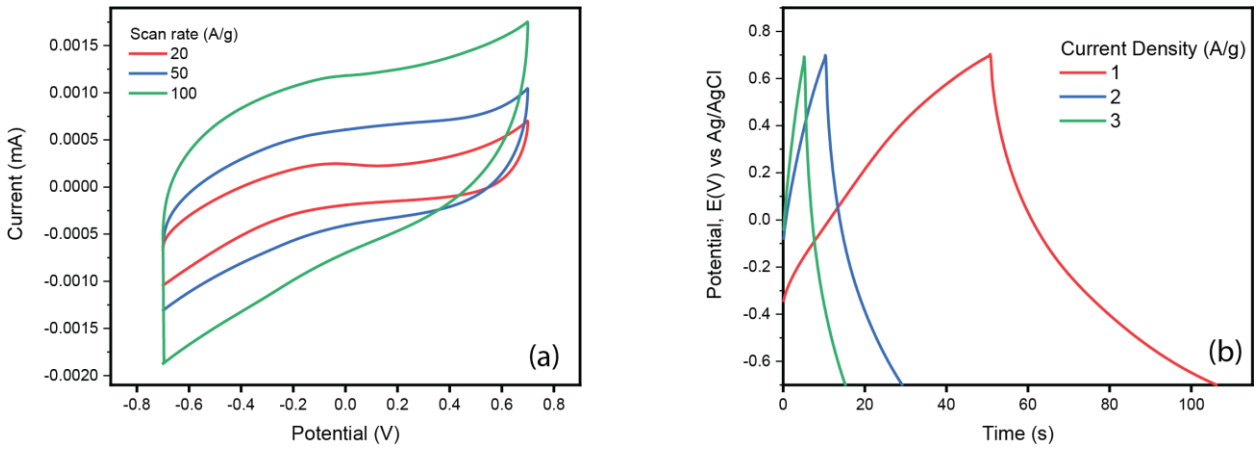

Figure 3. 1: Electrochemical capacitive behaviors of the AC studied using a three electrode system in CMC binder; (a) CVs at a different scan rate from 20 to 100 mVs^{-1}, (b) GCD curves at different current densities range from 1 to 3 A/g.

The capacitance performance of the prepared AC materials was further investigated using the GCD technique at different current densities of 1, 2, and 3 A/g using CMC binder. The shape of GCD curves was quasi-symmetrical and relatively triangular shape. The potential linear curve over time and nearlysymmetry triangle suggested less ideal behavior of the electrode material. As the value for current density decreased, the time for GCD increased..According to Liu et al. the slight curvature at low current density is due to the involvement of pseudocapacitance along with EDLC of the ACMG in CMC binder [20].

Table 3. 7: Specific capacitance at different current densities of ACMG in CMC

Current Density (A/g)	Specific Capacitance (F/g)
1	40.00
2	27.14
3	19.50

3.4.2 CV and GCD of ACMG in PVDF Binder

The CV curves of AC nanocomposite are shown in Figure 3.14 (a) within the potential range from -0.7 to + 0.7 V at different scan rates in PVDF binder. The quasi-rectangular shape of the CV curves without any obvious redox hump to the entire potential range. Wide rectangular CV curves with high current response were observed for all scan rates, defining the EDL nature of ACMG in PVDF, indicating its better electronic conductivity due to the easy movement of ions through the hierarchal and porous structure of AC [21]. Furthermore, it was also observed that the area enclosed by the CV curve increased with the increase of scan rate; the current show an increasing tendency indicating fast ion transportation and good capacitance retention of the

prepared sample ACMG in PVDF**.**The deviation rectangular shape of the CV curve at higher scan rates and potential may be attributing to the short, time-limited movement of electrolyte ions at the electrode surface.

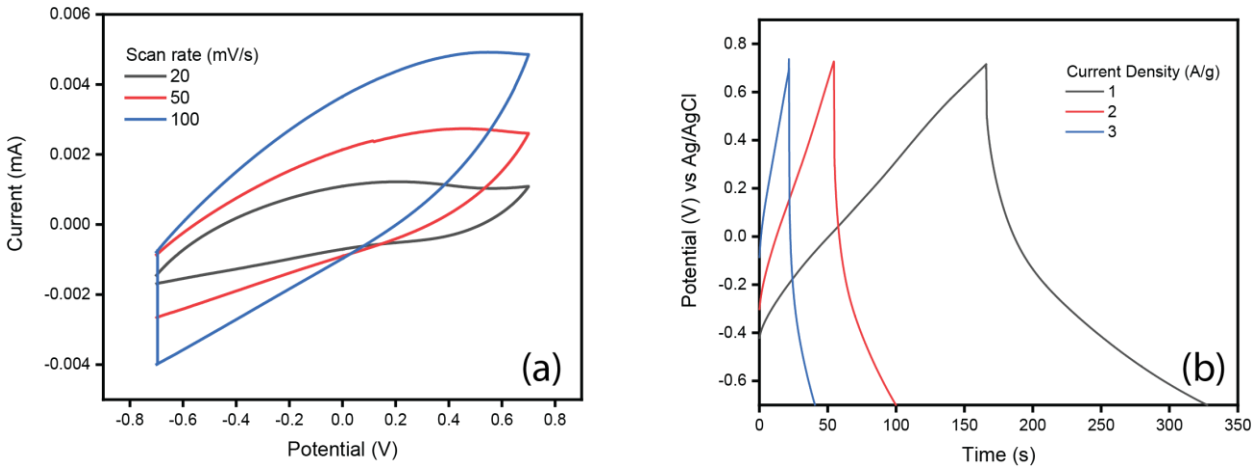

Figure 3. 13: Electrochemical capacitive behaviors of the AC studied using a three electrode system in PVDF binder; (a) CVs at a different scan rate from 20 to 100 mVs^{-1}, (b) GCD curves at different current densities range from 1 to 3 A/g.

To obtain more detailed information on the capacitance performance of the as-prepared AC-PVDF, GCD curves with various current densities were studied. GCD was performed within the potential window intimated from CV curves where no faradic process occurs. The GCD was conducted 1 to 3 Ag^{-1} to have the idea about the capacitive ability of the composites. All the curves show nearly symmetric behavior although at high current density the curves maintain linearity whereas at low current density the curves follow non-linear nature. The less symmetric GCDs are probably due to the combination of EDL and pseudocapacitance from the slight redox reaction of fluorinated PVDF binder [22]

Cs of AC-PVDF composites were determined from the GCD curves at different current densities. The Cs values are summarized in Table 3.8.

Table 3. 8: Specific capacitance at different current densities of ACMG in PVDF

Current Density (A/g)	Specific Capacitance (F/g)
1	115.00
2	65.71
3	40.71

3.4.3 CV and GCD of ACMG in PVA Binder

Figure 3.16 (a) represents the CVs of AC nanocomposite within the potential range from -0.7 to +0.7 V at different scan rates in PVA binder. The CV curve shows the almost symmetric rectangular shape within the potential range. Such curves indicate that the charge storage is dominated by EDL mechanism. However, it was also observed that the area enclosed by the CV curve increased with the increase of scan rate; the current show increasing tendency indicating fast ion transportation and good capacitance retention of the prepared sample in PVA [23]. Furthermore, curves show that with increasing scan rates the rectangular shape is not deformed that may for high porosity of nanostructure for adsorption and desorption electrolyte ions. It is also revealed that current density gradually increases with increasing scan rates, suggesting that the fabricated electrode with ACMG in the PVA binder exhibits high capacitive behavior for storing charges [24].

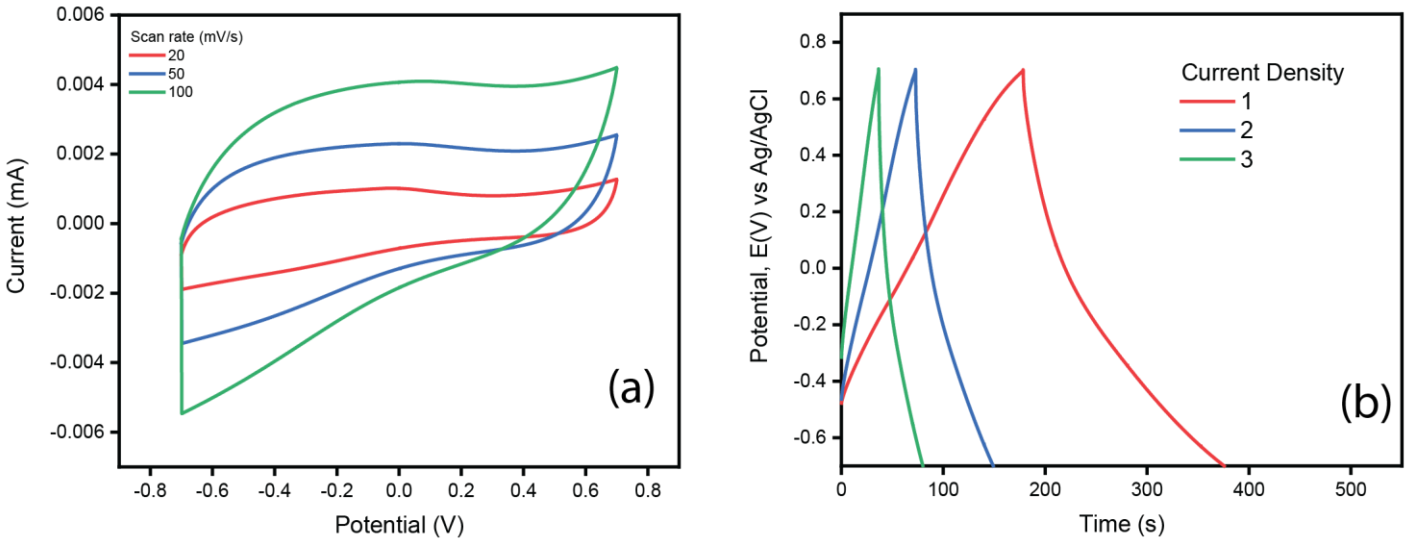

Figure 3. 14: Electrochemical capacitive behaviors of the AC studied using a three electrode system in PVA binder; (a) CVs at a different scan rate from 20 to 100 mVs^{-1}, (b) GCD curves at different current densities range from 1 to 3 A/g.

Further, GCD was also investigated for ACMG in PVA binder at different current densities. Figure 3.4.2 (b) illustrates the GCD curves of AC in PVA binder. These curves show a remarkable behavior at low current density within their non-faradic potential range and at higher current densities materials display good electrochemical performance as the GCD curves possess a triangular symmetry as well as linear slopes at higher current densities. Furthermore, the triangular shape of GCD with various current densities was retained event at high current density with high-rate capability and discharge time, indicating high chemical stability of AC-PVA [25].

The Cs of AC-PVA composites were calculated using GCD curves at varied current densities. The Cs findings are summarized in Table 3.9.

Table 3. 9: Specific capacitance at different current densities of ACMG in PVA

Current Density (A/g)	Specific Capacitance (F/g)
1	142.14
2	110.00
3	94.29

3.5 Comparative studies of electrochemical performances

3.5.1 CV and GCD of AC in CMC, PVDF, and PVA Binder

Figure 3.17 represents the cyclic voltammetric and galvanostatic charge-discharge response. CVs of the AC electrodes were performed between (-0.7 to + 0.7 V) in CMC, PVDF and PVA binder at various scan rates ranging from 20 to 100 mVs^{-1} as shown in 3.17 (b).

It is observed from this figure that the enclosed area by CV curves for AC-PVA is greater than the enclosed area by CV curves for AC-PVDF and AC-CMC. According to X. T. Chui et al. enclosed area of the CV curves is proportional to the charge storage capacity. Based on the observed results, it is logical to anticipate that the AC-PVA composite was responsible for the highest capacitance due to the bigger rectangular CV area and excellent ion accumulation.
This studies and investigations that these PVA composites have perfect capacitive characteristics as well as strong high-rate capabilities. The AC-PVA composite has a larger enclosed area than any other composites. From this point of view, another conclusion can be made that the capacitance of this composite should be higher than other CMC and PVDF composites.

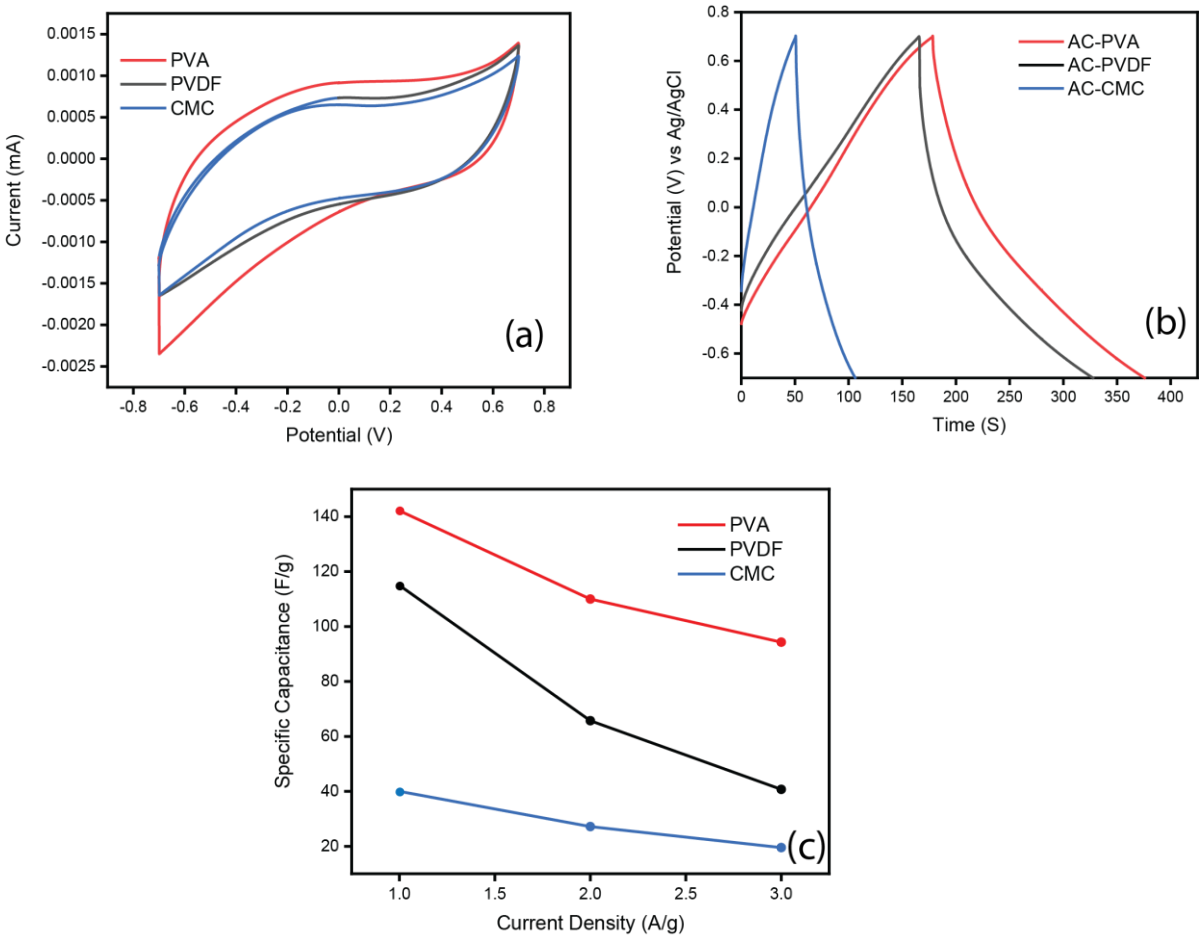

Figure 3. 15: Electrochemical capacitive behaviors of the AC studied using a two-electrode system in three different binders: in PVA, PVDF, and CMC. Comparison of (a) CV Curves at a fixed scan rate of 20 mVs^{-1}, (b) GCD curves at a fixed current density of 1 A/g, (c) C_{sp} (F/g) versus current density for the different binder of AC

The performance of the AC was further confirmed by the results of various GCD experiments carried out with the three different binders of the AC, and Figure 3.17 (b) shows a comparison of the GCD curves of the AC electrodes with the three different binders at a fixed current density of 1 A/g. The slope fluctuation of GCD curves shows the electrochemical adsorption and desorption from the electrode-electrolyte interface to the time dependence of potential. The GCD curves for PVA, PVDF, and CMC are symmetrical or triangular, indicating no noticeable potential drop (IR drop) and verifying the characteristic EDLC [26]. The AC has a longer discharge time, the most important and noticeable thing about this curve. The AC electrodes showed the discharge time was 56, 161, and 199 sec in the CMC, PVDF, and PVA at an applied current density of 1 A/g. As discharge time indicates the performance of a SC, the GCD results also show the superior performance of the AC in PVA. However, the higher voltage changes the capacitance of the electrode.

C_{sp} is an important parameter to consider for evaluating and comparing SC performances. It is often calculated from the GCD profiles of electrode materials of three-electrode systems. The C_{sp} values of the AC electrodes were calculated using eq (7) described in experimental section at different current densities in various binders (CMC, PVDF, and PVA) respectively. Plots of C_{sp}versus current density are shown in Figure 3.17 (c).The maximum C_{sp} values of the AC electrodes in CMC, PVDF, and PVA binders were 40, 115, and 142 F/g, respectively. This large difference between their capacitance values clearly reflected the successful execution of the idea of differentiating effective binders with a highly porous hierarchical carbon for high energy storage capacity [27]. This result indicates that the ACPVA composite exhibits a higher C_s has a high rate of capacitance, which is attributed to one of the most important electrochemical properties in the application of charge storing devices.

3.5.2 Determination of energy density and power density

Energy density and power density are two important factors to consider when using SCs in real-world applications, and they are usually shown in a Ragone plot [28]. The amount of energy that may be stored in a particular mass of a material, system, or area of space per unit volume is referred to as energy density. The more energy a system or substance stores in its mass, the higher its energy density. The fact that an object has a high energy density does not indicate how quickly it can be used. The power density of a material contains this information. Power density is a measurement of power output per unit volume and is defined as the quantity of power (time rate of energy transfer) per unit volume. It specifies the rate at which it may release energy. The formulas below were used to figure out the energy density (E) and power density (P) of AC samples in different binders.

$$E = 0.5 \times Csp(\Delta V)^2/3.6 \quad \text{.....} \quad (3.1)$$

$$P = E \times 3600/\Delta t \quad \text{.....} \quad (3.2)$$

The reported E and P values of AC produced from biomass sources are shown in Figure 3.18**.** The E values of the AC-CMC, AC-PVDF, and AC-PVA composites were 10.89, 31.31, and 38.7 Whkg-1, respectively, while the P values were 700 Wkg-1. These data further demonstrated the AC's superiority and revealed that the strain supercapacitor reagone in our designed device.

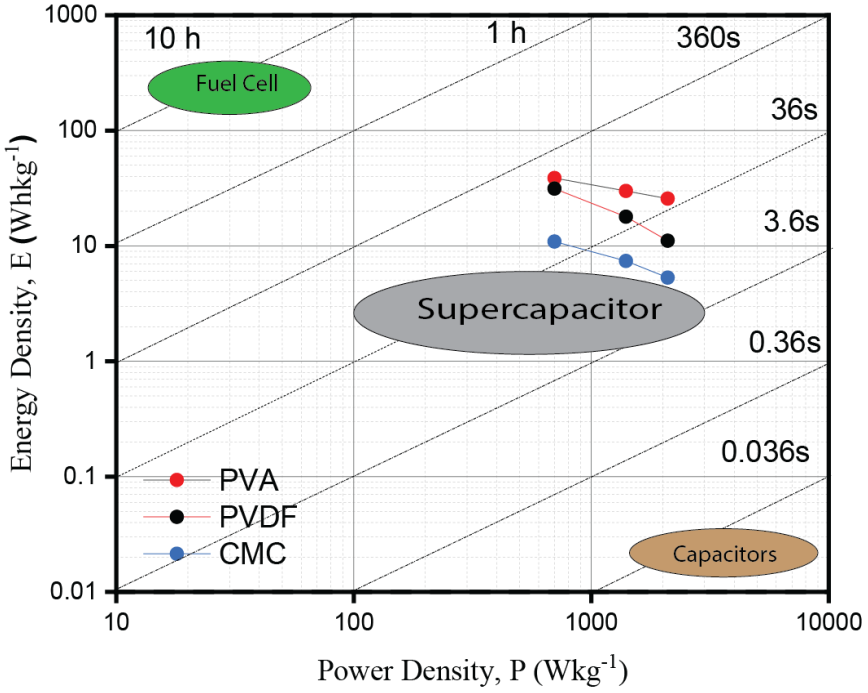

Figure 3. 16: Ragone plot for energy density and power density of AC in different polymeric binders.

3.5.3 EIS analysis

The ability of EIS to figure out the physical and electronic properties involved in electrochemical systems, such as diffusion coefficient, electron transfer rate constants, adsorption mechanisms, charge transfer resistances, corrosion properties, capacitances, and many others, has greatly increased in the last few decades [29].

EIS is presented by a Nyquist plot consisting of an imaginary part, $-Z_{Im}$, as a function of the real part, Z_{Re}, of the complex impedance of a double layer capacitor []. As mentioned in the experimental section, the obtained EIS data are presented by a Nyquist plot, and Figure 3.19 depicts a typical Nyquist plot in the frequency range of 0.01 Hz to 100 kHz. The supercapacitor electrodes with different binder showed a vertical Nyquist plot in the low-frequency region due to the Warburg impedance, suggesting good capacitive behavior. At mid-frequency, the small semi-circle measures the interfacial charge transfer resistance (R_{ct}) and the double-layer capacitance (C_{dl}) connected in parallel with each other. The first intersection points with the real axis in the high-frequency region measure the values of ohmic resistance of the electrolyte and the electrode material's internal resistance (R_s). The R_s values obtained from the supercapacitors were calculated at 4.0, 10.0, and 18.0 Ω for the AC with PVA, PVDF, and CMC, respectively. The yielded ESR value is 8, 17, and 28 Ω for the AC with PVA, PVDF, and CMC, indicating high electron conduction and fast ion exchange between the electrode and electrolyte for the AC with PVA binder. This result is due to the higher conductivity of AC electrodes with PVA. Also, AC electrodes with PVA showed a more vertical straight line perpendicular to the horizontal coordinate of the Nyquist plot, indicating the formation of more EDLC due to the highly porous

structure of the AC. This is further evidence that the AC-based supercapacitor with the PVA polymeric binder shows better capacitive behavior than the others.

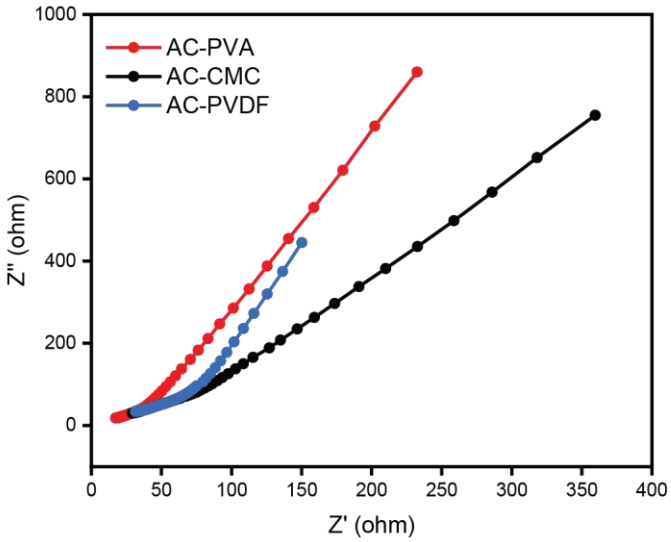

Figure 3. 17: Typical Nyquist plot of an AC modified graphite electrode in the frequency range of 100 kHz to 0.01 Hz at a potential of 10 mV in three different binders.

According to Figure 3.19, our Nyquist plots using EIS data will be fitted with a well-known Randles circuit (Circuit 1 in Figure 3.20), which comprises of a series resistance (Rs), a double layer capacitance (Cdl), a charge transfer resistance (Rct), and a Warburg resistance (Zw).

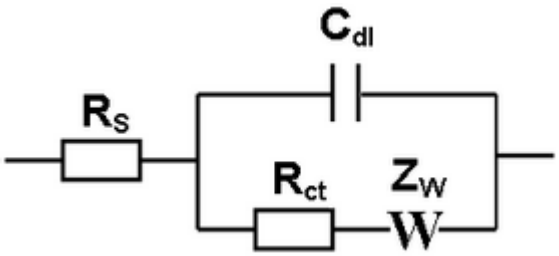

Figure 3. 18: Randles equivalent circuit

The porous nature of our synthesized carbonaceous materials and the roughness of our modified electrodes compelled us to introduce a pore capacitance 9Cp), a pore resistance (Rp), and a constant phase element (CPE) with the Randles circuit [30].

3.6 Cyclic Stability Analysis of the ACMG Electrode Using the Best Performed Binder

The Galvanostatic CD technique was employed to observe the cyclic stability test of the prepared AC-PVA composites.

Figure 3.19 shows the variation of capacitance retention and columbic efficiency with the increase in cycle number at a fixed current density of 10 Ag^{-1}. The GCD curve of the first (left) and last (right) 5 cycles of the GCD test of the AC-PVA for 10,000 cycles showed uniform structure retained after 1000 cycles, just like the first 5 cycles. After 1000 cycles, the repeated cyclic performance of the AC-based supercapacitor in the PVA binder undergoes a slight degradation in columbic efficiency and capacitance retention in 10,000 charge-discharge cycles. The AC-PVA retains 97% of columbic efficiency after 10,000 cycles with 80% of capacitance retention. The superior columbic efficiency is related to the high effectiveness of the AC-based supercapacitor for storing charges in the PVA binder [31]. The cycle stability of the composites may be attributed to the good conductivity of the composite with a highly porous structure and to the compact and definite semi-crystal structure of the PVA binder.

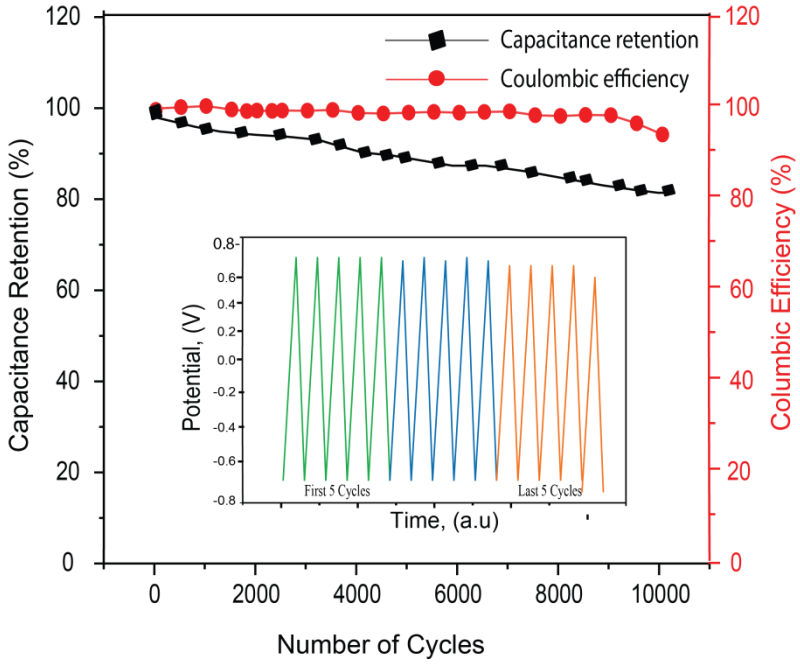

Figure 3. 19: Cyclic stability test of AC-PVA composites at 10 A/g current density.

3.7 Optimization of Binder

To evaluate the sepecific capacitance of the prepared nanomaterials more clearly, the electrodes with varying binders concentration within their permissible voltage window at 1 Ag^{-1} current density with different content of binders were applied to investigate by GCD method in 0.5 M Na_2SO_4 solution. The results showed in Table 10, suggest that the prepared nanomaterials exhibited different capacitive behavior with increasing binder wt%.

Table 3. 10: Variation of specific capacitances of AC electrodes with various contents of three binders at 1 A/g current density.

Binder	Current Density (A/g)	Binder Content (wt %)	C_{sp} (F/g)	Energy density (Wh kg^{-1})	Power density (W kg^{-1})
PVA	1	5	19	5.25	700
		10	142	38.7	700
		15	133	36.36	700
PVDF	1	5	14	3.89	700
		10	115	31.31	700
		15	107	29.16	700
CMC	1	5	7	1.95	700
		10	40	10.89	700
		15	31	8.56	700

For each binder, the specific capacitance of AC-PVA, AC-PVDF, and AC-CMC electrodes first increases with increasing binder concentration and then decreases with further expansion in the same experimental condition.In the cases of AC-PVA, AC-PVDF, and AC-CMC, the optimal binder content and maximum performance were observed at 10 wt%, as shown in Figure 3.21.
The decrease in capacitance value with increasing binder content is due to the more significant electrochemical resistance and low ions diffusion in the electrode-electrolyte interface. The thickness of the electrode increases as the binder amount increases. As a result, a longer ionic motion distance from the electrolyte to the inner region of the nanomaterials may be required in the lower mass loaded electrode. Alkali cations have enough time to reach the surface of nanomaterials for the lower mass loaded electrode due to its thin thickness in the range of applied current densities. As a result, the absorption/desorption process may proceed smoothly.

High capacitance is typically achieved via a thin layer of electrode coating; however, this is not always the case for commercial reasons. The diffusion of ions from the electrolyte may get access to practically all accessible pores of the electrode at low current densities with an adequate binder concentration, resulting in a complete insertion reaction and almost perfect capacitive behaviour [32, 33].

Thus proper optimization of mass loading is necessary for achieving the maximum performance of electrode materials.

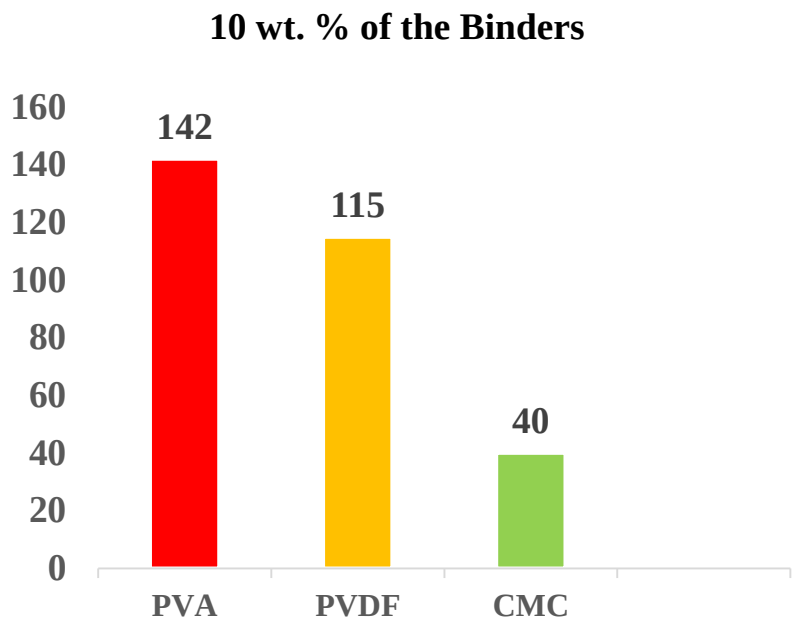

Figure 3. 20: Comparison of best optimal content (10 wt %) of three polymeric binders (PVA, CMC, and PVDF).

Finally, the findings reveal that supercapacitor performance varies depending on the binder content and the optimal content is 10 wt% to achieve the best electrochemical performance.

References:

[1] B. O. Muthén, "Beyond SEM: General Latent Variable Modeling," *Behaviormetrika*, vol. 29, no. 1, pp. 81–117, Jan. 2002.

[2] X. Geng, L. Li, and F. Li, "Carbon nanotubes/activated carbon hybrid with ultrahigh surface area for electrochemical capacitors," *Electrochimica Acta*, vol. 168, pp. 25–31, Jun. 2015, doi: 10.1016/j.electacta.2015.03.220.

[3] K. Rokosz, T. Hryniewicz, S. Raaen, D. Matýsek, Ł. Dudek, and K. Pietrzak, "SEM, EDS, and XPS Characterization of Coatings Obtained on Titanium During AC Plasma Electrolytic Process Enriched in Magnesium," *Adv. Mater. Sci.*, vol. 18, no. 3, pp. 68–78, Sep. 2018.

[4] V. Sinha and S. Chakma, "Synthesis and evaluation of CMC-g-AMPS/Fe/Al/AC composite hydrogel and their use in fluoride removal from aqueous solution," *Environ. Technol. Innov.*, vol. 17, p. 100620, Feb. 2020.

[5] R. Fateminia, S. Rowshanzamir, and F. Mehri, "Synergistically enhanced nitrate removal by capacitive deionization with activated carbon/PVDF/polyaniline/ZrO2 composite electrode," *Sep. Purif. Technol.*, vol. 274, p. 119108, Nov. 2021.

[6] S. R. Sandeman *et al.*, "Adsorption of anionic and cationic dyes by activated carbons, PVA hydrogels, and PVA/AC composite," *J. Colloid Interface Sci.*, vol. 358, no. 2, pp. 582–592, Jun. 2011.

[7] K. S. Lee, Y. J. Seo, and H. T. Jeong, "Capacitive behavior of functionalized activated carbon-based all-solid-state supercapacitor," *Carbon Lett.*, vol. 31, no. 5, pp. 1041–1049, Oct. 2021.

[8] E. Hastuti and I. Irfana, "Effect of PVDF composition in activated carbon derived from chicken feather on electrical properties," *J. Phys. Conf. Ser.*, vol. 1825, no. 1, p. 012052, Feb. 2021.

[9] D. M. Dhevi, A. A. Prabu, and K. J. Kim, "Infrared spectroscopic studies on crystalline phase transition of PVDF and PVDF/hyperbranched polyester blend ultrathin films," *Vib. Spectrosc.*, vol. 94, pp. 74–82, Jan. 2018.

[10] A. Noushini, B. Samali, and K. Vessalas, "Effect of polyvinyl alcohol (PVA) fibre on dynamic and material properties of fibre reinforced concrete," *Constr. Build. Mater.*, vol. 49, pp. 374–383, Dec. 2013.

[11] I. V. Pukhova, I. A. Kurzina, K. P. Savkin, O. A. Laput, and E. M. Oks, "Modification of polyvinyl alcohol surface properties by ion implantation," *Nucl. Instrum. Methods Phys. Res. Sect. B Beam Interact. Mater. At.*, vol. 399, pp. 28–33, May 2017.

[12] X. Wu *et al.*, "Effects of functional binders on electrochemical performance of graphite anode in potassium-ion batteries," *Ionics*, vol. 25, no. 6, pp. 2563–2574, Jun. 2019.

[13] H. Wang *et al.*, "A Universal Aqueous Conductive Binder for Flexible Electrodes," *Adv. Funct. Mater.*, vol. 31, no. 34, p. 2102284, Aug. 2021.

[14] S. Komaba, K. Shimomura, N. Yabuuchi, T. Ozeki, H. Yui, and K. Konno, "Study on Polymer Binders for High-Capacity SiO Negative Electrode of Li-Ion Batteries," *J. Phys. Chem. C*, vol. 115, no. 27, pp. 13487–13495, Jul. 2011.

[15] D. M. Hanson-Parr and T. P. Parr, "Thermal properties measurements of solid rocket propellant oxidizers and binder materials as a function of temperature," *J. Energ. Mater.*, vol. 17, no. 1, pp. 1–48, Mar. 1999.

[16] Z. Zhang, T. Zeng, Y. Lai, M. Jia, and J. Li, "A comparative study of different binders and their effects on electrochemical properties of LiMn 2 O 4 cathode in lithium ion batteries," *J. Power Sources*, vol. 247, pp. 1–8, Feb. 2014.

[17] A. Shafiepour, C. McCague, and M. Bahrami, "In-situ thermal conductivity of a sorption composite: An analytical approach," *Int. J. Heat Mass Transf.*, vol. 183, p. 122098, Feb. 2022.

[18] M. M. Shaijumon, F. S. Ou, L. Ci, and P. M. Ajayan, "Synthesis of hybrid nanowire arrays and their application as high power supercapacitor electrodes," *Chem. Commun.*, no. 20, p. 2373, 2008.

[19] R. Lin, P. L. Taberna, J. Chmiola, D. Guay, Y. Gogotsi, and P. Simon, "Microelectrode Study of Pore Size, Ion Size, and Solvent Effects on the Charge/Discharge Behavior of Microporous Carbons for Electrical Double-Layer Capacitors," *J. Electrochem. Soc.*, vol. 156, no. 1, p. A7, 2009.

[20] J. Huang *et al.*, "Polyaniline-intercalated manganese dioxide nanolayers as a high-performance cathode material for an aqueous zinc-ion battery," *Nat. Commun.*, vol. 9, no. 1, p. 2906, Dec. 2018.

[21] S. Xin, Y.-G. Guo, and L.-J. Wan, "Nanocarbon Networks for Advanced Rechargeable Lithium Batteries," *Acc. Chem. Res.*, vol. 45, no. 10, pp. 1759–1769, Oct. 2012.

[22] Z. Gao *et al.*, "Graphene incorporated, N doped activated carbon as catalytic electrode in redox active electrolyte mediated supercapacitor," *J. Power Sources*, vol. 337, pp. 25–35, Jan. 2017.

[23] C. Liu, G. Han, Y. Chang, Y. Xiao, M. Li, and W. Zhou, "Monolithic porous carbon derived from polyvinyl alcohol for electrochemical double layer capacitors," *Electrochimica Acta*, vol. 188, pp. 175–183, Jan. 2016.

[24] C.-C. Yang, S.-T. Hsu, and W.-C. Chien, "All solid-state electric double-layer capacitors based on alkaline polyvinyl alcohol polymer electrolytes," *J. Power Sources*, vol. 152, pp. 303–310, Dec. 2005.

[25] Md. Moniruzzaman, A. Akib, R. Shakil, S. Khatun, C. Kumar Roy, and A.-N. Chowdury, "Influence of Binder in the Fabrication of AC-Based High-Performance Electrochemical Supercapacitors," *ECS Trans.*, vol. 107, no. 1, pp. 18357–18365, Apr. 2022.

[26] Zulkifli, A., Saadiah, M.A., Mazuki, N.F., and Samsudin, A.S., "Characterization of an amorphous materials hybrid polymer electrolyte based on a LiNO3-doped, CMC-PVA blend for application in an electrical double layer capacitor.," *Mater. Chem. Phys.*, vol. 253, p. 123312, 2020.

[27] Xia, W., Mahmood, A., Zou, R., and Xu, Q., "Metal–organic frameworks and their derived nanostructures for electrochemical energy storage and conversion.," *Energy Environ. Sci.*, vol. 8, pp. 1837–1866, 2015.

[28] Chodankar, N.R., Bagal, I. V., Ryu, S.W., and Kim, D.H., "Hybrid material passivation approach to stabilize the silicon nanowires in aqueous electrolyte for high-energy efficient supercapacitor.," *Chem. Eng. J.*, vol. 362, pp. 609–618, 2019.

[29] Randviir, E.P., and Banks, C.E., "Electrochemical impedance spectroscopy: an overview of bioanalytical applications.," *Anal. Methods*, vol. 5, pp. 1098–1115, 2013.

[30] Pan, M., Zhang, D., Xu, X., Reda, A.T., and Li, J., "Efficient electrosorption of uranyl ions by a homemade amidoxime-modified carbon paper-based electrode in acidic aqueous

condition.," *J. Chem. Technol. Biotechnol.*, vol. 96, pp. 2916–2929, 2021.

[31] Yadav, N., Yadav, N., and Hashmi, S.A., "Ionic liquid incorporated, redox-active blend polymer electrolyte for high energy density quasi-solid-state carbon supercapacitor.," *J. Power Sources*, vol. 451, p. 227771, 2020.

[32] Winter, M., and Brodd, R.J., "What are batteries, fuel cells, and supercapacitors?," *Chem. Rev.*, vol. 104, pp. 4245–4269, 2004.

[33] Zhang, Z., Xiao, F., Qian, L., Xiao, J., Wang, S., and Liu, Y., "Facile Synthesis of 3D MnO2–Graphene and Carbon Nanotube–Graphene Composite Networks for High-Performance, Flexible, All-Solid-State Asymmetric Supercapacitors.," *Adv. Energy Mater.*, vol. 4, p. 1400064, 2014.

CHAPTER-4

CONCLUSION

Conclusion

The present study demonstrates a simple and cost-effective method for producing AC from banana leaves. FT-IR, SEM, and EDS studies characterize the composite formations. All of these procedures revealed that the intended materials had been produced effectively. Electrochemical studies such as cyclic voltammetry, galvanostatic charge-discharge, electrochemical impedance spectroscopy, and others were utilized to investigate the electrochemical response and applicability of the synthesized materials for supercapacitor technology.It is now widely acknowledged that polymer binders like carboxymethyl cellulose (CMC), polyvinyl alcohol (PVA), and polyvinylidene fluoride (PVDF) play significant roles, and the use of binders may block the pore and surface sites of the electrode modifier and thus influence the electrochemical performance of the supercapacitor device. So, several investigations were carried out to mitigate the abovementioned problems. Surprisingly, the synthesized AC with PVA reduced low specific capacitance difficulties compared to others. The AC shows the largest CV area and the highest specific capacitance in PVA. The formation of greater EDLC was seen in AC electrodes with PVA, which produced a more vertical straight line perpendicular to the horizontal coordinate of the Nyquist plot. In terms of the swelling test, PVA Shows low swelling properties compare to the others, which is responsible for high capacitance performance. In addition, for binder weight optimization, PVA shows the optimal content is 10 wt% to achieve the best electrochemical performance. Finally, the data suggest that PVA may be a superior binder for supercapacitors based on AC. The study's results could help develop a high-efficiency, environmentally friendly next-generation supercapacitor that can effectively handle the energy crisis.